Genetic and Circuit Mechanisms Underlying Natural Variation in Value-Based Decision Making

Dorsa Motevalli[1], Robert Alfredson[1], Sydney Fogleman[1], Emmanuel Medrano[1], William I. Silander[2,3,4], Toshihide Hige[2,3,4], Barry Dickson[5], Ulrich Stern[1], Chung-Hui Yang[1,6]

1. Dept. of Neurobiology, Duke University Medical School, Durham, NC 27710
2. Dept. of Biology, University of North Carolina, Chapel Hill, NC 27599
3. Dept. of Cell Biology and Physiology, University of North Carolina, Chapel Hill, NC 27599
4. Integrative Program for Biological and Genome Science, University of North Carolina, Chapel Hill, NC 27599
5. Queensland Neuroscience Institute, University of Queensland, St. Lucia, QLD 4067, Australia
6. Author of correspondence. Email: rebecca.yang@gmail.com

Summary

Genetically encoded differences in value-related functions are believed to influence decision biases in animals, yet direct causal evidence remains scarce. Here, we demonstrate how naturally occurring genetic variation between two *Drosophila* strains leads to distinct choices in an egg-laying-based decision-making task, where both sucrose and plain substrates are viable options. We identify a pair of long-range GABAergic neurons, Earmuff, that lower an option's intrinsic value and are both necessary and sufficient for shaping the flies' preferences. Further analysis reveals that expression-modifying single nucleotide polymorphisms (SNPs) within introns of the gene encoding the RNA-binding molecule *pumilio* (*pum*) – a known negative regulator of the voltage-gated sodium channel *NaV*$^{+}$ – exist between the two strains. These SNPs drive variation in *pum* expression within Earmuff, altering how each strain values the two substrates and biasing its decisions. Our findings establish a mechanistic link between genetic variation and the neural circuitry that governs value-based decision-making.

Introduction

Genomic information fundamentally shapes animal behavior by directing the structure, function, and adaptability of neural circuits. While many studies have shown that manipulating specific genes can alter behavior, some of the most exciting insights arise from research on natural genetic variation and its role in behavioral diversity. For example, natural differences in vasopressin receptor levels drive distinct pair-bonding behaviors in voles[1]; variation in the NPF receptor influences feeding behaviors in worms[2]; differences in bitter-taste receptors affect sugar bait responses in roaches[3]; and a recent finding revealing that variation in the enhancer controlling PDF peptide expression affects photoperiod adaptation in *Drosophila*[4]. These studies not only establish clear causal links between genes and behavior but also provide venues to determine how modifications in neural circuit properties can drive diverse behavioral adaptations.

Value-based decisions, where animals choose between alternatives based on their relative values, are likely shaped by genetic factors, too. Systems-level analyses of decision-making have identified key neural circuits involved in signaling option value. For example, dopaminergic (DA) neurons in the reward-sensitive ventral tegmental area (VTA) in rodents are activated by sucrose and salt – particularly under salt-deprived conditions[5,6], while neurons in the ventral pallidum (VP) encode the relative values of two palatable but differentially preferred sugars[7]. Additionally, neurons in the orbitofrontal cortex (OFC) in primates signal the subjective value of juice options[8]. Despite these insights, our understanding of how genetically encoded variations shape animals' "value functions" – and consequently their innate decision biases – remains limited. For instance, some animals might be genetically predisposed to prefer savory over sweet treats, while others exhibit the opposite preference; some may favor a hint of sourness in their sweets, while others dislike it. Addressing such questions requires identifying the casual genetic variations and determining how they alter the structure and function of the relevant value-encoding neural circuits.

Egg-laying site selection by *Drosophila* females has emerged as a powerful model for studying value-based decisions[9]. Females withhold egg-laying when no suitable substrate is available; but once a suitable substrate appears, they deposit eggs one at a time – searching, evaluating, and comparing options before each egg is laid[10,11]. Further, while common laboratory strains readily accept either a sucrose substrate (150 mM sucrose + 1% agarose) or a plain substrate (1% agarose) when only one type is offered, they robustly reject the sucrose option if both are available and within easy reach (Figure 1A-A")[10-13]. This suggests that, although a sucrose substrate is acceptable, it is valued less than the plain substrate. Such behavior illustrates flies' capacity to "choose the greater of two goods," a hallmark of value-based decisions. Further, recent work has identified the command neurons for egg-laying (oviDNs)[13], and recordings from these neurons as females deliberate where to lay an egg show a "ramp-to-threshold" activity pattern[14], reminiscent of the "drift-to-bound" dynamics observed in decision-relevant neurons in higher organisms[15,16]. Interestingly, different options induce different ramping speeds, reflecting their intrinsic values: the ramping is slower for sucrose and faster for the plain substrate[14]. Adding in *Drosophila*'s powerful molecular genetics, extensive circuit-monitoring and manipulation tools, and the recently completed full connectome of the female adult brain[17,18], egg-laying decisions in this model provide a unique opportunity to explore how genetic and circuit-level variations shape decision outcomes.

In this study, we leverage the naturally occurring differences in egg-laying preferences between a standard laboratory strain and a wild-caught African strain of *Drosophila*, along with a suite of genetic, genomic, and circuit imaging/manipulation tools, to investigate how genetic variations drive differences in decision-making behaviors through their effects on a value-assignment neural circuit. We find that differential expression of *pumilio* (*pum*), an RNA-binding molecule[19,20], is a

key genetic factor underlying these strains' distinct preferences. Specifically, strain-specific SNPs in the introns of *pum* modulate its expression, which in turn may influence the expression level of the voltage-gated sodium channel *paralytics* (*para*), causing a pair of value-assignment neurons that provide inhibitory input to the decision-making oviDNs to exhibit altered relative responses to sucrose versus plain options. Our study provides one of the first demonstrations of how natural genetic variation reshapes neural circuits, ultimately leading to unique decision biases.

Results

Identification of a pair of GABAergic projection neurons that is necessary for sucrose rejection and provides inhibitory input to the egg-laying decision center

We first identified circuit components that translate the sensory signals from the egg-laying options into value signals for use by the egg-laying decision center (i.e., oviDNs and their direct presynaptic inputs). A recent study has shown that sweet neurons on the legs are necessary and sufficient for the lower valuation of the sucrose substrate (150 mM sucrose in 1% agarose) relative to the plain one (1% agarose) in a sucrose vs. plain decision task[21] (Figure 1A-A'). In addition, a few pairs of recurrently connected neurons (e.g., oviENs) that output directly onto oviDNs have been reported[14] (Figure 1H). The circuit components that relay signal from the leg sweet neurons to the recurrently connected group presynaptic to oviDNs were not known, however. We thus conducted a small-scale screen focusing specifically on projection neurons that are anatomically positioned to relay information from the SEZ area (where the targets of the leg sweet neurons arborize) to the SLP area of the brain (where critical input into oviDNs such as oviENs arborize[13]). We inactivated several projection neurons that fit this morphological criterion by crossing the *split-GAL4* lines described in Sterne et al.[22] to the hyperpolarizing Kir2.1 channel[23] (Figure 1B). Using custom apparatuses each of which can assay sucrose vs. plain decision of 48 individual animals in parallel and custom code that can count eggs automatically (Figure 1A, Figure S1), we found that silencing the neurons labeled by one specific *split-GAL4* line consistently caused reduced sucrose rejection as compared to controls (Figure 1B, C); these neurons are named Earmuff, likely because the morphology of their axonal termini in the SLP areas are shaped like a pair of Earmuff (Figure 1D).

We next investigated the relationship between Earmuff, oviDNs, as well as the recurrently connected group presynaptic to oviDNs in the Flywire connectome[17] (Figure 1H). The first notable feature of Earmuff is that they are annotated to use GABA as transmitter in the Flywire connectome. To ascertain that Earmuff neurons are indeed GABAergic, we performed two experiments. First, we asked whether the promoter for the vesicular GABA transporter (vGAT), a molecular marker for GABAergic neurons, is active in Earmuff. We did this by asking if Earmuff can be co-labeled by *vGAT-LexA* (Figure 1E). Additionally, we also directly visualized the subcellular localization of the vGAT by examining a V5-tagged version of vGAT – knocked-in at the vGAT locus – whose expression can be turned on if the *GAL4* driver for Earmuff is active in GABAergic neurons[24]. Both experiments showed that Earmuff neurons are indeed GABAergic and that tagged vGAT were clearly enriched in the puncta at the presynaptic termini of Earmuff (Figure 1E, F & G). Aside from their identity as GABAergic inhibitory neurons, the second noteworthy feature of Earmuff is that they are annotated to directly signal both oviENs, the key excitatory input to oviDNs[14], and oviDNs (Figure 1H, I & J). Earmuff neurons provide the second strongest inputs to both oviENs and oviDNs (Figure 1H, I & J; Figure S2). It is worth mentioning that while oviENs and oviDNs are both absent in males, or at least not labeled by their respective drivers[13], Earmuff neurons are present in both sexes without obvious morphological differences between the two (Figure S6).

Taken together, we have identified a pair of long-range projection neurons that supply inhibitory input into the egg-laying decision center, and, critically, this inhibitory input is important for flies to reject the sucrose option over the plain one when given a choice between the two.

Activation of Earmuff neurons is sufficient to subtract value from a sugarless option

Having found that Earmuff neurons are necessary for sucrose rejection and supply inhibitory signal into the egg-laying decision center, we next asked if their activation is sufficient to promote rejection. To do so, we expressed the light-gated channel CsChrimson[25] in them and assessed how the flies would choose when given two plain substrates, one of which baited with red light. Specifically, we implemented a rule such that each time the fly enters the "light-baited" plain substrate, pulses of red light would be triggered to optogenetically activate Earmuff neurons (Figure 2B, C). This was implemented by using SkinnerSys, a high-throughput system we developed that allows us to track 40 individual animals in parallel (per apparatus) and deliver light to them in closed-loop[21] (Figure 2A). We found that *Earmuff>CsChrimson* (*CsC*) animals robustly rejected the plain option baited with light whereas controls flies were indifferent between the two options (Figure 2D, E), reminiscent of what we found with optogenetic stimulation of the leg sweet neurons[21].

To differentiate whether optogenetic activation of Earmuff neurons simply eliminates egg-laying – which could also explain the dramatically reduced egg-laying on the light-baited option – or whether such activation decreases the value of the option on which it occurs, we assessed how the flies behaved when both plain options were baited with closed-loop illumination (Figure 2F). If activation of these neurons simply eliminates egg-laying, the rate of egg-laying should be significantly reduced in *Earmuff>CsC* animals when compared to controls. If activation of these neurons devalues the option, however, the rate of egg-laying should not be significantly affected, similar to how the flies respond to the sucrose option: when two sucrose options are presented, they are accepted, but when sucrose is presented together with a plain option, sucrose is rejected[10]. We found that flies did not reduce their rate of egg-laying significantly when Earmuff activation was triggered on both plain options, in keeping with the notion that activation of Earmuff signals to reduce the relative value of an option as opposed to inhibiting egg-laying *per se* (Figure 2F).

Thus, our collective results so far support a simple model in which Earmuff neurons can act to reduce the value of an egg-laying option on which they are strongly activated, possibly by making the egg-laying decision-maker less excited by such an option, thereby leading to a preference for the option where Earmuff is less or not activated.

Earmuff neurons receive (indirect) input from sweet taste neurons and are differentially activated by plain and sucrose substrates

Next, we sought to test our model by examining Earmuff's response to sucrose and plain substrates. To begin, we addressed the possibility that these neurons are selectively activated by sweet taste, causing the sucrose option (1% agarose + sweet taste) to generate a stronger inhibitory signal to the decision-maker, leading to a lower perceived value compared to the plain option (1% agarose). We therefore tested if Earmuff neurons play a role in relaying sweet taste information gathered from the legs by assessing their relationship with the Taste Projection Neurons 2 (TPN2)[26]. We have previously shown that TPN2 neurons are functionally and anatomically connected to the leg sweet neurons in the VNC and are both necessary and sufficient to promote rejection of the sucrose option over the plain one[21] (Figure S3). Importantly, TPN2 neurons project their axons to the SEZ and SLP areas in the brain[21,26] (Figure 3B).

Are Earmuff neurons a target of TPN2 given the similarity in their behavioral role and the proximity of their dendritic and axonal processes, respectively, in the SEZ? Several lines of evidence suggest they indeed are. First, GRASP[27] experiment indicated that Earmuff and TPN2 make physical contacts in the SEZ (Figure 3A-C). Second, Ca^{2+} imaging experiments indicate that Earmuff neurons are activated by artificial stimulation of sweet neurons, as well as by exposure of the legs to sucrose solution (Figure S4).

To directly assess how Earmuff neurons respond to sucrose substrates (1% agarose + 150 mM sucrose) as opposed to sweet taste *per se*, we developed a preparation to monitor their Ca^{2+} response while simultaneously delivering the sucrose substrate to the legs of mated female flies (Figure 3D). Not surprisingly, Earmuff as well as their presynaptic partners TPN2 both responded clearly to the sucrose substrate, and Earmuff's response to sucrose decreased dramatically when output of TPN2 was inhibited (Figure 3 E, F and Figure S5). But curiously the response profiles of Earmuff and TPN2 differed slightly: while Earmuff sustained their response as long as the legs were in contact with substrates, TPN2 tended to decline more quickly while the legs were in still contact with the substrates (Figure 3E, F). Most interestingly, we found that Earmuff and TPN2 both responded clearly and consistently to the plain substrate (1% agarose), too, albeit at a much-reduced level (Figure 3E-F'). In contrast, neither group responded strongly to the presentation of a plastic surface (Figure 3E', F'). These results suggest that these neurons are not solely sensitive to sweet taste; rather, they integrate both taste and likely tactile information associated with an egg-laying option. This is in keeping with a recent connectome-based analysis showing that integration across modalities is a common theme of higher-order "taste neurons"[28]. Out of curiosity, we also tested how Earmuff and TPN2 in males and virgin females respond to substrates and found that, like their counterparts in mated females, they also responded significantly stronger to the sucrose substrate than to the plain one (Figure S6). But interesting differences do exist. For example, Earmuff neurons tended to elevate both their sucrose and plain responses in virgin females (Figure S6E, F). More intriguingly, Earmuff in males did not seem to respond to plain substrate at all (Figure S6H), while TPN2 did (Figure S6L), suggesting a potential male-specific top-down inhibitory input onto Earmuff.

So far, our collective results on the anatomical, physiological, and behavioral properties of Earmuff neurons suggest strongly that these inhibitory neurons (and their presynaptic partners TPN2) convey a signal akin to an innately specified "negative quality" associated with an egg-laying option. This mechanism enables the decision-maker to differentiate between two acceptable options with varying levels of negative quality. The sucrose substrate activates them strongly and is consequently valued less, while the plain substrate activates them mildly and is therefore valued more.

The strength of sucrose rejection varies among wild-caught strains and is governed by relatively simple genetic control

Having identified Earmuff neurons as key mediators of relative value assignment between sucrose and plain substrates in the standard lab strain (w^{1118}), we next investigated whether these neurons underlie (likely existing) natural variation in egg-laying choices among different wild-caught strains when presented with the same sucrose and plain options. We first conducted a survey of many wild-caught strains we obtained from the Cornell Stock Center. As expected, not all wild-caught strains rejected sucrose in favor of plain substrate, while we consistently observed such rejection in laboratory strains (e.g., w^{1118} and the various transgenes generated in similar background, including all the *split-GAL4s* and effector lines we employed for this study) (Figure 4A, B). In fact, only a minority of these strains showed a clear rejection of sucrose over plain; many were either indifferent towards or preferred sucrose substrate for egg-laying when given the same choice (Figure 4B). Notably, we did not detect any obvious correlation between rejection

strength and prominent geographical features. For example, one strain (line 51) that readily accepted sucrose was caught in South Africa, while another strain (line 128) with a comparable level of acceptance was caught in Maine, U.S.A. (Figure 4A, B).

To probe the genetic complexity underlying the sucrose preference exhibited by some of these strains, we next conducted a series of simple complementation tests and asked, for example, how the F_1 progenies of w^{1118} (the standard lab strain that rejects sucrose in a sucrose vs. plain task) and line 51 (the African strain that accepts sucrose in the same task) behave. Surprisingly, these F_1 progeny behaved much like w^{1118} and rejected sucrose over plain (Figure 4C), suggesting that sucrose acceptance is a recessive trait, while rejection is dominant. Further, the F_1 progeny from parents of two sucrose-accepting strains (51 and 128) rejected sucrose (Figure 4D). This result not only reinforces the recessive nature of the sucrose acceptance trait but also suggests that the "mutations" that are responsible for sucrose acceptance in these wild caught strains fall into at least two different complementation groups. These observations suggest that: 1) the genetic architecture that underlies the sucrose rejection/acceptance trait might be relatively simple and 2) the causal SNPs that drive varied levels of sucrose rejection could be mapped using a relatively straightforward approach. In this paper, we use the term SNPs in a broad sense to include both single nucleotide polymorphisms and indels (insertions and deletions).

SNP analysis of F_2 hybrids between laboratory WT (w^{1118}) and an African strain (line 51) identified variations in the regulatory region of *pum*, which encodes an RNA-binding protein, as potentially important for the sucrose acceptance/rejection trait

To map the relevant SNPs (and genes) responsible for driving the distinct valuation of the sucrose substrate by w^{1118} and line 51, we created animals whose genome was a hybrid of these two strains. Specifically, we backcrossed the F_1 female progeny of w^{1118} x line 51 crosses to line 51 males so that each individual F_2 female contained one intact, non-recombinant chromosome from line 51 and the other a recombinant mixture of line 51 and w^{1118} (Figure 5A). We then assayed the sucrose vs. plain egg-laying decision of many F_2 females, selected 192 individuals for full-genome sequencing, and performed a GWAS using PLINK[29] to identify SNPs associated with sucrose acceptance (Figure 5B, C). Three of the significant SNPs that came out of our analysis were particularly interesting because they are located within the introns of the same gene: *pumilio* (*pum*), a gene that encodes an RNA-binding protein (Figure 5D, Table S1)[19,20].

Given the recessive nature of the sucrose acceptance trait, we speculated that the three SNPs we identified in the *pum* locus of line 51 might reduce *pum* expression. This is because recessive mutations tend to be caused by reduced- or loss-of-function alleles. To test this, we performed two experiments. First, we assessed *pum* expression and found its level was indeed lower in the brains of line 51 than controls (e.g., $51/w^{1118}$) (Figure 5E). Second, we asked whether line 51 would fail to complement loss-of-function *pum* mutations by assessing the behavior of F_1 progeny of line 51 and different *pum* mutants. This was a direct test for a causal role of reduced *pum* in driving sucrose acceptance. We found that while F_1 progeny from control crosses (pum/w^{1118} and $51/w^{1118}$) rejected sucrose, *pum/51* accepted sucrose; importantly, this was true for three different *pum* alleles from different genetic backgrounds (Figure 4C and 5F).

Taken together, our analyses strongly suggest that *pum* level is crucial for how animals assign value to sucrose vs. plain options when making egg-laying decisions. Specifically, *pum* expression is higher in w^{1118}, promoting sucrose rejection, and lower in line 51, leading to sucrose acceptance.

Earmuff neurons' ability to differentiate between sucrose vs. plain substrates is reduced when *pum* expression is reduced

We have so far demonstrated that the inhibitory Earmuff neurons play a critical role in assigning value to sucrose vs. plain options, as does the level of *pum* expression. Next, we were curious whether the ability of Earmuff neurons to assign different values to sucrose vs. plain might change when *pum* expression is reduced. To do so, we assessed the substrate response of Earmuff neurons in w^{1118}*/pum* (controls) and the *51/pum* (surrogate for *51/51*) flies by introducing the driver and GCaMP reporter into them. Given inhibiting Earmuff neurons and reducing *pum* level both led to increased sucrose acceptance, we initially expected that Earmuff neurons might reduce their response to sucrose substrates in *51/pum* animals. To our surprise, however, we found that the response of Earmuff neurons to the sucrose substrate did not differ significantly between *51/pum* and w^{1118}*/pum* (Figure 6A, C; Figure S7), but Earmuff's response to the plain substrate increased significantly in *51/pum* (Figure 6B, D). This result suggests that reducing *pum* expression indeed reduces Earmuff neurons' ability to differentiate between the sucrose and plain options (Figure 6E), but it achieves this "leveling" not by reducing Earmuff's sucrose response but by increasing their plain response. Thus, *51/pum* animals increased their sucrose acceptance in a sucrose vs. plain task not because the sucrose option becomes more valuable but because the plain option loses its relative value.

Cell-autonomous reduction of *pum* or an increase in *para* in Earmuff or their presynaptic partners contributes significantly to sucrose acceptance

Next, we were curious about where reduced *pum* expression might exert its impact on Earmuff. In principle, *pum* might affect the response property of neurons that are presynaptic to Earmuff, and/or directly influence Earmuff neurons. To test the first scenario, we examined the response of TPN2 to sucrose vs. plain substrates in the same genetic backgrounds in which we tested the response of Earmuff. Similar to what we observed with Earmuff, TPN2's response to sucrose substrate did not change significantly between *51/pum* and w^{1118}*/pum*, whereas its response to plain increased (Figure 6F-J; Figure S7). This result suggests changes in Earmuff neuron responses are at least partly due to altered substrate responses in (presynaptic) TPN2.

To address the possibility that *pum* might also affect Earmuff in a cell-autonomous manner, we first used RNAi against *pum* to knock down its expression in Earmuff neurons specifically. Interestingly, overexpressing *pum*-RNAi in Earmuff led to a mild but statistically significant reduction in sucrose rejection (Figure 7A). In keeping with this behavioral phenotype, overexpressing *pum-RNAi* in Earmuff neurons increased their response to the plain substrate but did not significantly impact their response to the sucrose substrate (Figure 7C-E, Figure S7). Further, given that reduced *pum* in Earmuff *increased* their plain response, and that *paralytics* (*para*), the sole voltage-gated sodium channel (NaV^+) in flies, is known to be directly downregulated by *pum*[30,31], we were curious if increasing *para* expression in Earmuff neurons might mimic the impact of decreasing *pum* expression in them. And indeed, animals overexpressing *para* specifically in their Earmuff neurons increased their sucrose acceptance (Figure 7A). Further, this was accompanied by an increased ratio of Earmuff's response to plain vs. sucrose substrates, reminiscent of what we observed when we reduced *pum* in them (Figure 7F-H, Figure S7). A closer look at these responses revealed a notable difference between overexpressing *para* and reducing *pum* expression, however: while manipulating *pum* selectively increased Earmuff's plain response, overexpressing *para* increased Earmuff's response to both substrates but the increase in plain response was larger than the increase in sucrose response (Figure 7E, H, Figure S7). Further, cell-autonomous manipulation of *pum* and *para* specifically in TPN2, the presynaptic partner of Earmuff, showed similar results, consistent with the phenotype of TPN2 we observed in *pum/51* background (Figure 7I-N, Figure S7).

Taken together, our collective results suggest a model (Figure 8) that reduced *pum* expression in the TPN2 → Earmuff pathway contributes significantly to the sucrose acceptance phenotype exhibited by the African strain line 51. This reduction in *pum* weakens the ability of TPN2 – and more importantly, Earmuff neurons – to differentiate between the sucrose and the plain substrates, likely through upregulation of the voltage-gated sodium channel Para, thereby narrowing these two substrates' relative value.

Discussion

In this work, we identified a causal link between naturally occurring genetic differences (SNPs in *pum*) and natural variation in the outcome of a value-based decision in *Drosophila*, as well as one relevant neural substrate through which the genetic differences influence decision-making. We found that while our standard laboratory strain rejects a sucrose-containing option over a plain one when selecting sites for egg-laying, a wild-caught strain from Africa (line 51) accepts sucrose when given the same task. Leveraging the discovery that sucrose acceptance in the African strain is a recessive trait, we next found that, through SNP mapping of F_2 hybrids, reduced expression of *pum*, a gene encoding an RNA-binding molecule, is responsible this strain's sucrose acceptance. In parallel, we identified a pair of inhibitory Earmuff neurons as one "decision-critical" neural substrate whose function is impacted by *pum* expression. These inhibitory neurons signal the negative value/quality associated with an option and are necessary and sufficient to promote the rejection of an inferior option. They are more activated by the (inferior) sucrose substrate than the plain one in the standard lab strain. Critically, their ability to differentiate between the two substrates diminishes in the African strain, contributing to increased sucrose acceptance in this strain. The altered response of Earmuff in the African strain likely has two origins: cell-targeted reduction of *pum*, possibly accompanied by an increase in *para*, within these neurons, as well as similar changes in their presynaptic partner, TPN2. These results suggest that variations in choice preference in other organisms, including humans, may in part stem from genetically encoded variations in value-assignment circuits.

Is reduced *pum* expression the sole cause for the African strain's altered relative valuation of sucrose vs. plain substrates? Most likely it is not. Several SNPs associated with other genes were also statistically significant (Table S1), although we have not tested their functional roles. Further, while *pum/51* trans-heterozygous animals exhibit significantly increased sucrose acceptance as compared to both parental controls, their phenotype was not always as strong as that of line 51 homozygous animals. Similarly, while our results show that altered substrate responses of TPN2 and Earmuff neurons play a critical role in driving the altered decision outcomes when *pum* expression was reduced, other decision-critical neurons may also be impacted. For example, we have not thoroughly tested the impact of altered *pum* and *para* on neurons postsynaptic to Earmuff, such as oviENs, or on dopaminergic (DA) neurons, which are reciprocally connected to oviENs[14] and may signal the *positive* value/quality associated with an option. Several lines of evidence suggest that a sucrose-sensitive, value-adding pathway operates in parallel to the value-subtracting Earmuff pathway. For example, when we silenced the leg and esophagus sweet neurons labeled by *Gr64a-GAL4*[21], the flies switched to preferring sucrose over plain substrates. This and additional findings suggest that some labellar sweet neurons may enhance the relative value of the sucrose substrate over the plain one[21], possibly signaling some of the oviEN-innervating excitatory neurons, such as the DA neurons mentioned earlier. And, if so, an enhanced response of this pathway to sucrose may also contribute to the increased sucrose acceptance observed in the African strain.

How does *pum* reduction lead to selective enhancement of the plain response in Earmuff and TPN2? One intriguing aspect of our findings is that reducing *pum* expression – either in whole animals or in just the TPN2 or Earmuff neurons – increased the response of these neurons to the

plain substrate but not to the sucrose substrate. One possibility is that Pum proteins are more enriched at these neurons' connections with neurons that signal the presence of plain substrate (e.g., some mechanosensitive and/or water-sensing neurons) compared to their connections with the neurons that signal the sucrose substrate. As such, *pum* reduction might selectively lead to increased local translation of Na^+V – and possibly other relevant targets – at these synapses, thereby selectively enhancing the excitability of these neurons to plain substrates. Verifying this idea requires the identification of the relevant inputs onto TPN2 and Earmuff neurons, as well developing tools to examine Pum levels and Pum's ability to repress *NaV*$^+$ translation at subcellular resolution. Earmuff neurons in males may also provide a useful test case for this idea. These neurons respond only to the sucrose substrate, possibly because Pum is hyper-enriched in their connection with the plain-signaling pathway, drastically reducing the NaV^+ protein levels at these synapses.

Lastly, is down-regulation of *pum* a common theme underlying increased sucrose acceptance in the various wild-caught strains we observed? While we are still at the early stages of characterizing these strains, two findings are already noteworthy. First, the key "mutations" driving increased sucrose acceptance of line 128 must be different from those in line 51 since the two lines genetically complemented each other: that is, the F_1 progeny of line 128 and line 51 rejected the sucrose option while both parents were indifferent or slightly preferred sucrose (Figure S8). Curiously, however, *pum* expression in line 128 was also reduced as compared to lab strain. This suggests that although the relevant phenotype-causing SNPs in line 128 do not reside in the *pum* locus, they likely occur in genes that directly or indirectly regulate *pum* expression. Second, we found that several of the sucrose-accepting strains failed to complement both line 128 and line 51 (Figure S8), suggesting that these strains harbor phenotype-causing SNPs from both lines, making it highly likely that they also exhibit reduced *pum* expression. These results suggest that adjusting *pum* levels, albeit through different molecular mechanisms, may be a general strategy for increasing sucrose acceptance. It will be interesting to sequence the *pum* locus in the various lines that failed to complement line 51 to determine if they harbor SNPs in *pum* different from those found in line 51. If so, these results suggest that the regulatory regions of *pum* serve as "hotspots" for selective pressures driving sucrose acceptance. While we do not yet fully know why some strains prefer sucrose while others reject it, it is conceivable that the presence of sucrose poses certain threats, though severity of such threats may vary across geographical locations.

Methods

Fly husbandry

Flies were reared on molasses-based food and maintained in a 25°C incubator with 60% humidity. For most behavior and imaging experiments, we used mated females that were 6-14 day old. For experiments where we used RNAi to knock down gene expression, flies were aged up to 22 days to allow sufficient time for targeted mRNA to be depleted. See the table of (abbreviated) crosses used for the flies used for each experiment.

Immunostaining

Brains and ventral nerve cords (VNCs) were dissected and fixed in 4% paraformaldehyde prepared in PBS containing 0.3% Triton X-100 (PBST). The dilution factors for the antibodies used in this study were as follows: NC82: 1:50, anti-GFP: 1:1000, anti-RFP: 1:5000, anti-V5: 1:500, donkey anti-mouse Cy3: 1:500, donkey anti-mouse Alexa Fluor 488: 1:500, donkey anti-rabbit Alexa Fluor 594: 1:500, and donkey-anti rabbit Alexa Fluor 488: 1:500. Samples were imaged using a Zeiss LSM700 with either a 20x air objective or a 40x oil objective and the acquired confocal images were then post-processed with Fiji.

RT-qPCR

RNA Extraction: Female fly brains (n = 30) or heads (n = 15) were dissected in RNase-free PBS and transferred to TRIzol reagent. RNA was extracted using the Qiagen RNeasy Kit and Qiagen Shredder column, following the manufacturer's protocol. DNase treatment: To remove genomic DNA contamination, samples were treated with TURBO DNase™. RNA concentration was measured using the Qubit RNA High Sensitivity Assay Kit. cDNA Synthesis: cDNA was synthesized from total RNA using the SuperScript™ IV First-Strand Synthesis System, following the manufacturer's instructions. Reverse transcription quantitative PCR (RT-qPCR): We used QuantStudio3 to perform qPCR using TaqMan™ Fast Advanced Master Mix, following the manufacturer's protocol. Gene expression levels were assessed using TaqMan Gene Expression Assays with Dm02361909_s1 (act5C, housekeeping gene) and Dm02135527_m1 (*pum*, gene of interest.0

Full genome sequencing SNP analysis

DNA extraction: We extracted DNA from individual F2 recombinants using a standard protocol[32]. Whole genome sequencing: We used SNPsaurus and Novogene to perform whole genome sequencing of a total of 192 of the selected F2 recombinants. SNPsaurus and Novogene sequenced 96 flies each using Illumina NovaSeq sequencers, with paired-end reads of 159 bp and 150 bp, respectively, and coverages of 10x and 20x, respectively. Variant calling pipeline. We implemented our own GATK-based variant (SNP and indel) calling pipeline to turn the raw reads (FASTQ files) into a VCF file that gives the variant calls for each fly. The pipeline used GATK tools when available, but we preferred fastp to MarkIlluminaAdapters to take advantage of fastp's adapter auto-detection. We also wrote a Python script to run pipelines in parallel, making efficient use of modern CPUs' many cores. For both the pipeline and the script, we strove for low SSD wear. Our pipeline produced by-sample GVCF files, which we combined into a single "cohort" VCF file for all 192 flies. We filtered out genotype calls in the VCF file with genotype quality (GQ) below 13, corresponding to 5% call error probability. GWAS using PLINK. The goal of our GWAS using PLINK[29] was to identify variants associated with sucrose acceptance. We used the flies' preference index (PI) both as quantitative trait and to group flies into "sucrose accepting" and "sucrose rejecting" flies (case/control phenotype). For the group-based analysis, we ran the analysis twice with different thresholds – first for groups "PI≥-0.1" and "PI≤-0.75" (with 49 and 82 flies, respectively) and then for groups "PI≥0" and "PI≤-0.80" (with 38 and 73 flies, respectively). We used PLINK's max(T) permutation procedure with 5 million permutations and Fisher's exact

test to calculate multiple-comparison-corrected empirical p-values (EMP2). We next performed a quantitative trait analysis using PI as a continuous variable. From this analysis, we specifically selected the genomic control-corrected p-values (GC) and the Bonferroni-corrected p-values (BONF). Table S1 shows the 19 variants from the cohort VCF file that were significantly associated ($p \leq 0.05$) with sucrose acceptance or PI for each of the 4 p-values – EMP2 (one for each grouping), GC, and BONF. To identify genes potentially affected by each of the 19 variants, we used SnpEff, and the rightmost column in Table S1 shows those genes and the relative location of the variant.

Egg-Laying Assay (standard)

Preparation of flies to be used for assay: We used our standard "egg-laying deprivation" protocol previously described[33]. Briefly, we grouped 35 females with ~10-15 males in a food vial supplemented with yeast paste (live yeast granules mixed with 0.5% propionic acid) for 4 days. This was to induce females to produce and maintain many eggs in an environment that lacks a good surface for egg-laying due to excess of larvae by day 4. As such, females will readily lay eggs when placed in our custom chambers (apparatuses). Preparation of egg-laying substrates: We prepared the substrates right before dispensing individual females (deprived following the protocol we just stated) into our custom chambers. The sucrose substrates were made by diluting an aliquot of 2M stock solution into 1% agarose (e.g., 750 μl into 10 ml of 1% agarose) while the plain substrates were made diluting the same amount of ddH_2O into 1% agarose. We routinely keep a bottle of pre-melted 1% agarose in a 55 °C water bath. After being loaded into the chambers, flies are covered and incubated at 25 °C with 60% humidity for egg-laying. Egg counting: After allowing flies to lay eggs for 18–20 hours ("overnight"), we took pictures of the bottom plate (see Figure 1) and then used our (custom-built) automatic egg counter to segment arenas and count the eggs laid in each trough (code available at https://github.com/rcalfredson/Eggsactly). The tool is a web-based application that automatically quantifies eggs in each agarose region from an overhead photograph of a multi-fly egg-laying chamber. After the user uploads an image, a neural network detects the circular hole at the center of each fly enclosure (arena) and uses these holes as anchor points to define segmentation boxes around the two agarose regions at opposite ends of each arena. Each agarose region is then cropped into its own subimage, which is passed to a second neural network trained to detect individual eggs. Finally, the user can review the automatically identified eggs, correct counts if needed, and download the results either as a CSV (with egg counts per agarose region) or as a fully annotated image. Calculation of Preference Index (PI): We then calculated the preference index (PI) for each animal using the following formula: (# of eggs on sucrose − # of eggs on plain)/(total # of eggs). This index reflects the relative preference for sucrose over plain agarose. Importantly, if a given fly laid fewer than 10 eggs, its PI was omitted for analysis – we adopted the view that flies' preferences are clearer if they had laid at least 10 eggs.

Egg-laying assay (optogenetics)

Fly and chamber preparations: Female flies were prepared and their egg-laying PI was calculated as in the non-optogenetics case, but in the optogenetics case vials were kept in darkness and the food was supplemented with 200 mM all-trans-retinal to allow CsChrimson to be activated by light. Additionally, plain agarose substrates were supplemented with 100 mM sorbitol to ensure flies had access to nutrition during the assay. Egg-laying assay: Flies were loaded into arenas under dim lighting conditions and were allowed to lay eggs overnight (>14 hours) in the SkinnerSys setup, a high-throughput closed-loop stimulation platform. The setup included several custom components optimized for tracking and stimulation: 1) SkinnerTrax: Custom software for real-time tracking of multiple flies while delivering light pulses to individual flies based on their behaviors[34] (code available at https://github.com/ulrichstern/SkinnerTrax); 2) Modified two-choice arenas with shorter and slightly angled sidewalls; 3) LED stimulation setup: A custom printed circuit board (PCB) equipped with 80 individually controllable red (624 nm) Cree LEDs, with two LEDs per

arena for uniform illumination. 4) Apparatus stand: a custom-designed stand held the arenas, cameras (Microsoft LifeCam Cinema), and PCB in fixed positions. A dimmed light pad (Artograph LightPad A920) provided low-intensity backlighting for tracking without activating channelrhodopsins. Cameras were fitted with blue-pass filters (LEE Filters 172 Lagoon Blue) to reduce the pulsing red LEDs' impact on tracking. Stimulation protocol: Optogenetic stimulation was applied only when SkinnerTrax detected that a fly was positioned over the agarose substrate of interest. The LEDs for that arena were pulsed at 2 Hz (250 ms on/off), providing approximately 6.8 μW/mm² of red light during "LED on."

Calcium Imaging

Preparation: Each fly was anesthetized individually on a CO_2 pad, and the head was positioned through an opening in an aluminum foil plate. UV-cured glue was applied to immobilize its wings and thorax, while the eyes and proboscis were also secured. The head was then submerged in 1X standard imaging buffer[21] freshly supplemented with 4 mM $CaCl_2$. A small section of the cuticle was carefully removed, to expose the region of the interest. An additional 100 μL of 1X imaging solution with 4 mM $CaCl_2$ was applied to facilitate imaging with a water immersion objective. Image acquisition: Imaging was performed at 25°C using a ZEISS LSM700 laser confocal microscope equipped with a 40X water immersion objective, at 128 x 128 pixels and 8 fps. Stimulation protocol for substrate contacts: During imaging, agarose with 150 mM sucrose or plain agarose was presented to the fly's legs for about 60 seconds using a micromanipulator. Each substrate was presented in alternating order three times with about 30 second of no substrate in between agarose presentations. Stimulation protocol for solution contacts: To acclimate the fly's legs to moisture, 100 μL of DI water was first applied, ensuring that subsequent response to the sucrose solution would be specifically due to sugar detection by the leg chemosensory receptors rather than a response to moisture. Following this acclimation step, 50 μL of 450 mM of either sucrose or sorbitol was added to the 100 μL of DI water in which the fly's legs were submerged. Fluorescence quantification and analysis: Raw LSM files were first uploaded to an in-house application for motion correction to improve accuracy of fluorescence measurements. Regions of interest (ROIs) were defined in ImageJ to measure fluorescence intensity. For Earmuff neurons, the ROI was drawn around the soma in each hemisphere, while for TPN2 neurons, the ROI encompassed the arbors within the SEZ region. For oviDN and oviEN neurons, the ROI was drawn in the SMP region of the brain. Baseline fluorescence (F_0) for each substrate was determined from four to ten time points immediately preceding leg contact with the substrate, depending on the experiment. Fluorescence values (F(t)) were then measured, and the change in fluorescence (ΔF/F) was calculated using the formula: $\Delta F/F = (F(t) - F_0) / F_0$. ΔF/F values were calculated over the entire duration of substrate contact and averaged across three trials for each substrate condition.

Statistics

All statistical tests, except the SNP analysis, were performed using GraphPad Prism 10. Sample sizes are stated in the figure legends. Unless mentioned otherwise, each dot in a swarm plot and each sample represents a biological replicate (an individual fly). For Ca^{2+} imaging, we typically averaged responses from three technical replicates for the same fly to give one sample (e.g., Fig. 3E'). Bars and whiskers indicate mean and 95% confidence interval (CI). Similarly, ΔF/F graphs show mean and 95% CI bands (e.g., Fig. 3E). Also, we used unpaired *t*-tests with Welch's correction to compare two samples, except for 3E' and F' where paired t-tests were used, and one-way ANOVA (with Tukey's multiple comparison test) to compare three or more samples. To assess whether a sample mean was different from 0, we used one-sample t-tests. The following notation is used to indicate significance: ns: not significant, ****: $p < 0.0001$, ***: $p < 0.001$, **: $p < 0.01$, and *: $p < 0.05$.

Key resource table

Reagent/Resource	Source	Identifier
Antibodies		
NC82 (mouse)	DSHB	AB_2314866
Anti-RFP (rabbit)	ThermoFisher	AB_560939
Donkey anti-mouse, Alexa-488	ThermoFisher	AB_141607
Donkey anti-rabbit, Alexa-594	ThermoFisher	AB_141637
Donkey anti-rabbit, Alexa-488	ThermoFisher	AB_2535792
Donkey anti-mouse, Cy3	Jackson ImmunoResearch	AB_2340813
Anti-GFP (rabbit)	ThermoFisher	AB_221569
Anti-V5 (mouse)	ThermoFisher	AB_2556564
Oligonucleotides		
pumillio	Thermofisher	Dm02135527_m1
actin5C	Thermofisher	Dm02361909_s1
Chemicals		
Sucrose	Sigma Aldrich	S0389-5KG
UltraPure Agarose	Invitrogen	16500500
All trans Retinal	Sigma Aldrich	R2500-100MG
UltraPure™ DNase/RNase-Free Distilled Water	ThermoFisher Scientific	10977023
Active dry yeast	VWR	75860-348
Potassium Chloride	Sigma-Aldrich	P9541-1KG
SlowFade™ Diamond Antifade Mountant	ThermoFisher	S36963
RNase A, DNase and protease-free	ThermoFisher	EN0531
RNaseZap	ThermoFisher	AM9780
10X PBS	Invitrogen	AM9624
DEPC-Treated Water	ThermoFisher	AM9920
RNAlater	Sigma-Aldrich	R0901
TRIzol Reagent	Invitrogen	15596026
Ethyl alcohol	Sigma-Aldrich	E7023
2-Mercaptoethanol	Sigma-Aldrich	M6250
QIAshredder	Qiagen	79654
RNeasy Mini Kit	Qiagen	74106
SuperScript™ IV First-Strand Synthesis System	ThermoFisher	18091050
TaqMan™ Fast Advanced Master Mix for qPCR	ThermoFisher	4444557
Molasses food	Archon Scientific, Inc.	B70101
Qubit DNA HS Assay kit	Invitrogen	Q32854
Qubit RNA HS Assay kit	Invitrogen	Q32855
TURBO DNA-free Kit	Invitrogen	AM1907

Fly strains		
w^{1118}		
TPN2-GAL4 (regular)	Kim et al.[26]	
TPN2-ss-GAL4	Gift from Barry Dickson	SS66351
Earmuff	Janelia	SS31063
Tophat (1)	Janelia	SS39993
Tophat (2)	Janelia	SS39932
Peafowl	Janelia	SS37792
Amulet	Janelia	SS32423
Sullivan	Janelia	SS42639
Bobber	Janelia	SS29032
Turner	Janelia	SS49422
Kelp	Janelia	SS43885
Hound	Janelia	SS47232
UAS>STOP>KIR-eGFP	Watanabe et al.[35]	
Otd-FLP	Asahina et al.[36]	
UAS>stop>CsChrimson^{tdt}	Watanabe et al.[35]	
Vgat-LexA	BDSC	BL-84441
Gad-LexA	BDSC	BL-94893
UAS-Kir2.1	Baines et al.[23]	
Empty-ss-GAL4	BDSC	BL-79603
UAS-CsCrimson^{venus}	BDSC	BL-55136
UAS-CsChrimon^{tdT} *(x)*	Gift from Toshi Hige	
lexA-CsChrimson^{tdt} *(x)*	Gift from Toshi Hige	
TPN2-LexA	Gift from Barry Dickson	VT-057358-LexA
LexA-FLP	BDSC	BL-55819
LexA-CsChrimson^{venus}	BDSC	BL-55139
GRASP (*spGFPs*)	BDSC	BL-64315
UAS-GCaMP6f	BDSC	BL-52869
UAS-GCaMP6s	BDSC	BL-42746
Ohau, Hawaii (Line 0)	Cornell Stock Center	14021-0231.00
Mysore, India (Line 06)	Cornell Stock Center	14021-0231.06
Captain Cook, Hawaii (Line 54)	Cornell Stock Center	14021-0231.54
Guam (Line 198)	Cornell Stock Center	14021-0231.198
Kuala Lumpur, Malaysia (Line 04)	Cornell Stock Center	14021-0231.04
Cape Town, South Africa (Line 51)	Cornell Stock Center	14021-0231.51
Vinasco, Mexico (Line 42)	Cornell Stock Center	14021-0231.42
Coffs Harbour, Australia (Line 18)	Cornell Stock Center	14021-0231.18
Le Reduit, Mauritius (Line 53)	Cornell Stock Center	14021-0231.53
pum allele	BDSC	BL-6782
pum allele	BDSC	BL-97221
pum allele	BDSC	BL-25480
UAS-pum-RNAi	BDSC	BL-38241
UAS-para	Piggott et al.[37]	

UAS-GCaMP8m	BDSC	BL-92592
UAS-GCaMP7b	BDSC	BL-79029
oviEN-ss-GAL4	*Janelia*	SS65426
oviDN-ss-GAL4	*Janelia*	SS46540
UAS-TNT	BDSC	BL-28996
Gr5a^{LexA}	BDSC	BL-93440
Gr64f^{LexA}	BDSC	BL-93445
UAS-syt-eGFP	BDSC	BL-33065
Software		
Automatic egg counter	In-house	https://github.com/rcalfredson/Eggsactly
SkinnerSys	In-house	https://github.com/ulrichstern/SkinnerTrax
Motion-correction app	In-house	Based on NoRMCorre[38]
Prism 10	GraphPad	
ImageJ/Fiji	https://imagej.nih.gov/ij/	

Table of crosses used to generate the flies in each figure

Figure 1	Abbreviated Crosses
B	*Empty-ss-GAL4 x UAS-Kir* *Tophat x UAS-Kir* *Tophat_II x UAS-Kir* *Peafowl x UAS-Kir* *Amulet x UAS-Kir* *Earmuff x UAS-Kir* *Sullivan x UAS-Kir* *Bobber x UAS-Kir* *Turner x UAS-Kir* *Kelp x UAS-Kir* *Hound x UAS-Kir*
C	*Earmuff x UAS>stop>Kir* *Earmuff x otd-FLP* *Earmuff x otd-FLP; UAS>Stop>Kir*
D	*UAS-CsChrimson*^{tdt}*; Earmuff X w*^{1118}
E-G	*UAS>stop>GFP; Earmuff x vGAT-LexA; LexA-FLP*
Figure 2	
E, F	*Empty-ss-GAL4 x UAS-CsChrimson*^{Venus}
	Earmuff x UAS-CsChrimson^{Venus}
Figure 3	
A	*UAS-CsChrimson*^{tdt}*; Earmuff x w*^{1118}
B	*TPN2-LexA x LexA-CsChrimson*^{Venus}
C	*Earmuff x TPN2-LexA; spGFPs*
E, E’	*Earmuff x UAS-GCaMP6f*
F, F’	*TPN2-ss-GAL4 x UAS-GCaMP6s*
Figure 4	

B	*w^{1118}* *14021-0231.00* (Oahu, Hawaii) *14021-0231.06* (Mysore, India) *14021-0231.54* (Captain Cook, Hawaii) *14021-0231.198* (Guam) *14021-0231.04* (Kuala Lumpur, Malaysia), aka *04* *14021-0231.158* (Montpellier, France) *14021-0231.57* (Summerhaven, Arizona) *14021-0231.51* (Cape Town, South Africa), aka *51* *14021-0231.128* (Southwest Harbor, Maine), aka *28* *14021-0231.42* (Vinasco, Mexico), aka *42* *14021-0231.18* (Coffs Harbour, Australia)
C	*w^{1118}* *51* *w^{1118} x 51*
D	*128* *51* *128 x 51*
Figure 5	
B	*51/51* x *w^{1118}/51*
E	*51 x 51* *w^{1118} x 51* *51 x pum* (BL-6782) *w^{1118} x pum* (BL-6782)
F	*w^{1118} x pum* (BL-6782) *51 x pum* (BL-6782) *51 x pum* (BL-97221) *51 x pum* (BL-25480)
Figure 6	
A-E	*UAS-GCaMP8m; Earmuff^{AD}/CyO; Earmuff^{DBD}, pum$^{BL-6782}$/TM2 x w^{1118}* *UAS-GCaMP8m; Earmuff^{AD}/CyO; Earmuff^{DBD}, pum$^{BL-6782}$/TM2 x 51*
F - J	*UAS-GCaMP6s/CyO; TPN2-GAL4, pum$^{BL-6782}$/TM6b x w^{1118}* *UAS-GCaMP6s/CyO; TPN2-GAL4, pum$^{BL-6782}$/TM6b x 51*
Figure 7	Abbreviated crosses
A	*Earmuff x UAS-pum-RNAi* *Empty-ss-GAL4 x UAS-pum-RNAi*
	Earmuff X UAS-para *Earmuff X w^{1118}*
B	*TPN2-ss-GAL4 x UAS-pum-RNAi* *Empty-ss-GAL4 x UAS-pum-RNAi*
	TPN2-ss-GAL4 x UAS-para *Empty-ss-GAL4 x UAS-para*
C, D & E	*UAS-GCaMP8m; Earmuff x w^{1118}* *UAS-GCaMP8m; Earmuff x UAS-pum-RNAi*
F, G & H	*UAS-GCaMP8m; Earmuff x w^{1118}* *UAS-GCaMP8m; Earmuff x UAS-para*
I, J & K	*TPN2-ss-GAL4 x UAS-GCaMP7b* *TPN2-ss-GAL4* x *UAS-pum-RNAi; GCaMP7b*
L, M & N	*UAS-GCaMP6s; TPN2-GAL4 x w^{1118}*

	UAS-GCaMP6s; TPN2-GAL4 x UAS-para
Figure S2	
A, B	*UAS-TNT; Earmuff x UAS-GCaMP8s; oviEN* *UAS-TNT; Empty-ss-GAL4 x UAS-GCaMP8s; oviEN*
C, D	*UAS-TNT; Earmuff x UAS-GCaMP8s; oviDN* *UAS-TNT; Empty-ss-GAL4 x UAS-GCaMP8s; oviDN*
Figure S3	
A	*UAS-CsChrimson^{tdt}; TPN2-ss-GAL4 x w^{1118}*
B	*UAS>stop>GFP; TPN2-ss-GAL4 x hs-FLP*
C	*TPN2-ss-GAL4 x Gr5a^{LexA}; spGFPs*
D	*UAS>stop>GFP; TPN2-ss-GAL4 x TPN2-LexA; LexA-FLP*
E	*TPN2-LexA, UAS>stop>Kir; LexA-FLP x TPN2-ss-GAL4*
F	*TPN2-ss-GAL4 x UAS-GCaMP6s*
G	*LexA-CsChrimson^{tdt}; UAS-GCaMP6s; Gr64f^{LexA} x TPN2-ss-GAL4*
Figure S4	
A, A’	*Earmuff x UAS-GCaMP6f*
B	*lexA-CsChrimson^{tdt}; Gr5a-lexA; UAS-GCaMP6f x Earmuff* *lexA-CsChrimson^{tdt}; UAS-GCaMP6f x Earmuff*
Figure S5	
A	*TPN2-ss-GAL4 x UAS-syt*
B	*Earmuff x UAS-syt*
C, D	*UAS-GCaMP8m; Earmuff x UAS-TNT; TPN2-ss-GAL4* *UAS-GCaMP8m; Earmuff x UAS-TNT; Empty-ss-GAL4*
Figure S6	
A, B, & C	*otd-FLP, UAS>stop>CsChrimson^{tdt} x Earmuff*
D	*TPN2-lexA; Sp-GFPs x Earmuff*
E-H, M	*Earmuff x UAS-GCaMP6f*
I-L, N	*TPN2-ss-GAL4 x UAS-GCaMP6s*
Figure S7	
A	*UAS-GCaMP8m;Earmuff^{AD}; Earmuff^{DBD}, pum$^{BL-6782}$/TM2 x w^{1118}* *UAS-GCaMP8m;Earmuff^{AD}; Earmuff^{DBD}, pum$^{BL-6782}$/TM2 x 51*
B	*UAS-GCaMP8m; Earmuff x w^{1118}* *UAS-GCaMP8m; Earmuff x UAS-pum-RNAi*
C	*UAS-GCaMP8m; Earmuff X w^{1118}* *UAS-GCaMP8m; Earmuff X UAS-para*
D	*UAS-GCaMP6s; TPN2-GAL4, pum$^{BL-6782}$ x w^{1118}* *UAS-GCaMP6s; TPN2-GAL4, pum$^{BL-6782}$ x 51*
E	*TPN2-GAL4^{AD}, UAS-GCaMP7b; TPN2-GAL4^{DBD} x w1118* *TPN2-GAL4^{AD}, UAS-GCaMP7b; TPN2-GAL4^{DBD} x UAS-pum-RNAi*
F	*UAS-GCaMP6s; TPN2-GAL4 x w^{1118}* *UAS-GCaMP6s; TPN2-GAL4 x UAS-para*
Figure S8	Abbreviated crosses
A	*128* *51* *128 x 51*
B	*04* *51* *04 x 51*

C	*04* *128* *04 x 128*
D	*42* *51* *42 x 51*
E	*42* *128* *42 x128*

Acknowledgements

We would like to thank the Bloomington Stock Center for providing fly strains and the Duke Physics Shop for fabricating the behavior apparatuses. We would also like to thank members of the Yang Lab for their comments and suggestions, especially Ned (Suyang) Kan for his help with developing the preparation to image substrate-induced neuronal responses. We would also like to thank Dr. Arnaldo Rosario for his insights on *pum*. This work was supported by an invertebrate neuroscience research grant to C.-H.Y. and by grants from NIH/NIDCD (R01DC018874) and NSF (2034783) to T.H.

Author contributions

D.M., U.S., and C.-H.Y. designed the project. D.M. performed the bulk of the behavioral and imaging experiments and analyzed the data. S.F., D.M., and E.M. performed complementations and RT-qPCR experiments and analyzed the data. W.S. and T.H. contributed to the initial Ca^{2+} responses of Earmuff. B. D. provided key reagent and insight on TPN2. U.S. built the behavior-dependent stimulation system. U.S. performed the SNP analysis using initial work by R.A. R.A. wrote the code for the automatic egg-counting tool. C.-H.Y. wrote the initial draft of the paper, which was then edited by D.M., E.M., T.H., and U.S.

Competing interests

The authors declare no competing interests.

References

1. Lim, M.M., Wang, Z., Olazabal, D.E., Ren, X., Terwilliger, E.F., and Young, L.J. (2004). Enhanced partner preference in a promiscuous species by manipulating the expression of a single gene. Nature *429*, 754-757. 10.1038/nature02539.
2. de Bono, M., and Bargmann, C.I. (1998). Natural variation in a neuropeptide Y receptor homolog modifies social behavior and food response in C. elegans. Cell *94*, 679-689. 10.1016/s0092-8674(00)81609-8.
3. Wada-Katsumata, A., Silverman, J., and Schal, C. (2013). Changes in taste neurons support the emergence of an adaptive behavior in cockroaches. Science *340*, 972-975. 10.1126/science.1234854.
4. Shahandeh, M.P., Abuin, L., Lescuyer De Decker, L., Cergneux, J., Koch, R., Nagoshi, E., and Benton, R. (2024). Circadian plasticity evolves through regulatory changes in a neuropeptide gene. Nature *635*, 951-959. 10.1038/s41586-024-08056-x.
5. Cone, J.J., Fortin, S.M., McHenry, J.A., Stuber, G.D., McCutcheon, J.E., and Roitman, M.F. (2016). Physiological state gates acquisition and expression of mesolimbic reward prediction signals. Proc Natl Acad Sci U S A *113*, 1943-1948. 10.1073/pnas.1519643113.

6. Liu, W.W., and Bohorquez, D.V. (2022). The neural basis of sugar preference. Nat Rev Neurosci *23*, 584-595. 10.1038/s41583-022-00613-5.
7. Ottenheimer, D., Richard, J.M., and Janak, P.H. (2018). Ventral pallidum encodes relative reward value earlier and more robustly than nucleus accumbens. Nat Commun *9*, 4350. 10.1038/s41467-018-06849-z.
8. Padoa-Schioppa, C., and Assad, J.A. (2006). Neurons in the orbitofrontal cortex encode economic value. Nature *441*, 223-226. 10.1038/nature04676.
9. Cury, K.M., Prud'homme, B., and Gompel, N. (2019). A short guide to insect oviposition: when, where and how to lay an egg. J Neurogenet *33*, 75-89. 10.1080/01677063.2019.1586898.
10. Yang, C.H., Belawat, P., Hafen, E., Jan, L.Y., and Jan, Y.N. (2008). Drosophila egg-laying site selection as a system to study simple decision-making processes. Science *319*, 1679-1683. 10.1126/science.1151842.
11. Vijayan, V., Wang, Z., Chandra, V., Chakravorty, A., Li, R., Sarbanes, S.L., Akhlaghpour, H., and Maimon, G. (2022). An internal expectation guides Drosophila egg-laying decisions. Sci Adv *8*, eabn3852. 10.1126/sciadv.abn3852.
12. Yang, C.H., He, R., and Stern, U. (2015). Behavioral and circuit basis of sucrose rejection by Drosophila females in a simple decision-making task. J Neurosci *35*, 1396-1410. 10.1523/JNEUROSCI.0992-14.2015.
13. Wang, F., Wang, K., Forknall, N., Patrick, C., Yang, T., Parekh, R., Bock, D., and Dickson, B.J. (2020). Neural circuitry linking mating and egg laying in Drosophila females. Nature *579*, 101-105. 10.1038/s41586-020-2055-9.
14. Vijayan, V., Wang, F., Wang, K., Chakravorty, A., Adachi, A., Akhlaghpour, H., Dickson, B.J., and Maimon, G. (2023). A rise-to-threshold process for a relative-value decision. Nature *619*, 563-571. 10.1038/s41586-023-06271-6.
15. Shadlen, M.N., and Kiani, R. (2013). Decision making as a window on cognition. Neuron *80*, 791-806. 10.1016/j.neuron.2013.10.047.
16. Shadlen, M.N., and Newsome, W.T. (1996). Motion perception: seeing and deciding. Proc Natl Acad Sci U S A *93*, 628-633. 10.1073/pnas.93.2.628.
17. Dorkenwald, S., Matsliah, A., Sterling, A.R., Schlegel, P., Yu, S.C., McKellar, C.E., Lin, A., Costa, M., Eichler, K., Yin, Y., et al. (2024). Neuronal wiring diagram of an adult brain. Nature *634*, 124-138. 10.1038/s41586-024-07558-y.
18. Scheffer, L.K., Xu, C.S., Januszewski, M., Lu, Z., Takemura, S.Y., Hayworth, K.J., Huang, G.B., Shinomiya, K., Maitlin-Shepard, J., Berg, S., et al. (2020). A connectome and analysis of the adult Drosophila central brain. Elife *9*. 10.7554/eLife.57443.
19. Wharton, R.P., Sonoda, J., Lee, T., Patterson, M., and Murata, Y. (1998). The Pumilio RNA-binding domain is also a translational regulator. Mol Cell *1*, 863-872. 10.1016/s1097-2765(00)80085-4.
20. Zamore, P.D., Williamson, J.R., and Lehmann, R. (1997). The Pumilio protein binds RNA through a conserved domain that defines a new class of RNA-binding proteins. RNA *3*, 1421-1433.
21. Chen, H.L., Motevalli, D., Stern, U., and Yang, C.H. (2022). A functional division of Drosophila sweet taste neurons that is value-based and task-specific. Proc Natl Acad Sci U S A *119*. 10.1073/pnas.2110158119.
22. Sterne, G.R., Otsuna, H., Dickson, B.J., and Scott, K. (2021). Classification and genetic targeting of cell types in the primary taste and premotor center of the adult Drosophila brain. Elife *10*. 10.7554/eLife.71679.
23. Baines, R.A., Uhler, J.P., Thompson, A., Sweeney, S.T., and Bate, M. (2001). Altered electrical properties in Drosophila neurons developing without synaptic transmission. J Neurosci *21*, 1523-1531. 10.1523/JNEUROSCI.21-05-01523.2001.

24. Certel, S.J., McCabe, B.D., and Stowers, R.S. (2022). A conditional GABAergic synaptic vesicle marker for Drosophila. J Neurosci Methods *372*, 109540. 10.1016/j.jneumeth.2022.109540.
25. Klapoetke, N.C., Murata, Y., Kim, S.S., Pulver, S.R., Birdsey-Benson, A., Cho, Y.K., Morimoto, T.K., Chuong, A.S., Carpenter, E.J., Tian, Z., et al. (2014). Independent optical excitation of distinct neural populations. Nat Methods *11*, 338-346. 10.1038/nmeth.2836.
26. Kim, H., Kirkhart, C., and Scott, K. (2017). Long-range projection neurons in the taste circuit of Drosophila. Elife *6*. 10.7554/eLife.23386.
27. Feinberg, E.H., Vanhoven, M.K., Bendesky, A., Wang, G., Fetter, R.D., Shen, K., and Bargmann, C.I. (2008). GFP Reconstitution Across Synaptic Partners (GRASP) defines cell contacts and synapses in living nervous systems. Neuron *57*, 353-363. 10.1016/j.neuron.2007.11.030.
28. Walker, S.R., Pena-Garcia, M., and Devineni, A.V. (2024). Connectomic analysis of taste circuits in Drosophila. bioRxiv. 10.1101/2024.09.14.613080.
29. Chang, C.C., Chow, C.C., Tellier, L.C., Vattikuti, S., Purcell, S.M., and Lee, J.J. (2015). Second-generation PLINK: rising to the challenge of larger and richer datasets. Gigascience *4*, 7. 10.1186/s13742-015-0047-8.
30. Mee, C.J., Pym, E.C., Moffat, K.G., and Baines, R.A. (2004). Regulation of neuronal excitability through pumilio-dependent control of a sodium channel gene. J Neurosci *24*, 8695-8703. 10.1523/JNEUROSCI.2282-04.2004.
31. Muraro, N.I., Weston, A.J., Gerber, A.P., Luschnig, S., Moffat, K.G., and Baines, R.A. (2008). Pumilio binds para mRNA and requires Nanos and Brat to regulate sodium current in Drosophila motoneurons. J Neurosci *28*, 2099-2109. 10.1523/JNEUROSCI.5092-07.2008.
32. Huang, A.M., Rehm, E.J., and Rubin, G.M. (2009). Quick preparation of genomic DNA from Drosophila. Cold Spring Harb Protoc *2009*, pdb prot5198. 10.1101/pdb.prot5198.
33. Gou, B., Zhu, E., He, R., Stern, U., and Yang, C.H. (2016). High Throughput Assay to Examine Egg-Laying Preferences of Individual Drosophila melanogaster. J Vis Exp, e53716. 10.3791/53716.
34. Stern, U., Srivastava, H., Chen, H.L., Mohammad, F., Claridge-Chang, A., and Yang, C.H. (2019). Learning a Spatial Task by Trial and Error in Drosophila. Curr Biol *29*, 2517-2525 e2515. 10.1016/j.cub.2019.06.045.
35. Watanabe, K., Chiu, H., Pfeiffer, B.D., Wong, A.M., Hoopfer, E.D., Rubin, G.M., and Anderson, D.J. (2017). A Circuit Node that Integrates Convergent Input from Neuromodulatory and Social Behavior-Promoting Neurons to Control Aggression in Drosophila. Neuron *95*, 1112-1128 e1117. 10.1016/j.neuron.2017.08.017.
36. Asahina, K., Watanabe, K., Duistermars, B.J., Hoopfer, E., Gonzalez, C.R., Eyjolfsdottir, E.A., Perona, P., and Anderson, D.J. (2014). Tachykinin-expressing neurons control male-specific aggressive arousal in Drosophila. Cell *156*, 221-235. 10.1016/j.cell.2013.11.045.
37. Piggott, B.J., Peters, C.J., He, Y., Huang, X., Younger, S., Jan, L.Y., and Jan, Y.N. (2019). Paralytic, the Drosophila voltage-gated sodium channel, regulates proliferation of neural progenitors. Genes Dev *33*, 1739-1750. 10.1101/gad.330597.119.
38. Pnevmatikakis, E.A., and Giovannucci, A. (2017). NoRMCorre: An online algorithm for piecewise rigid motion correction of calcium imaging data. J Neurosci Methods *291*, 83-94. 10.1016/j.jneumeth.2017.07.031.

Figure legend

Figure 1. Identification of a pair of GABAergic projection neurons that are necessary for sucrose rejection and send inhibitory input to the egg-laying decision center
(A) Above: schematic diagram of a single egg-laying arena we used to assess sucrose (S) vs. plain (P) egg-laying decisions. Below, our apparatus that can assay egg-laying decisions of 48 individual females. **(A')** Sample image of egg-laying decisions of 24 individual females. Since the image is for illustration only, the genotypes of the flies are not pertinent. **(A")** Preference index (PI) we used to quantify each fly's preference for S when deciding between S and P; it is calculated as follows: (**#** of eggs on S – **#** of eggs on P)/ total # of eggs laid.
(B) A *split-GAL4* screen we performed to identify neurons that affect PI when silenced with Kir.
(C) Validation of the impact of silencing Earmuff neurons on PI.
(D) Confocal image of Earmuff neurons (green) in the brain.
(E) Confocal image showing that Earmuff can also be labeled/intersected by *vGAT-lexA*.
(F) Confocal image of Earmuff processes (inside the red rectangle in panel **E**) in the superior lateral protocerebrum (SLP).
(G) Confocal image showing the presence of vGAT proteins (red) colocalized as yellow puncta at the termini of Earmuff (green).
(H) Schematic representation of the anatomic connectivity between Earmuff neurons, oviENs, and oviDNs based on reconstruction from Flywire. Red arrows indicate direct inhibitory inputs, green arrows indicate direct excitatory inputs, and black arrows represent indirect connections. Numbers next to each connection denote the total number of synapses (summing, e.g., the synapses of three oviENs per hemisphere).
(I) Input neurons to oviDNs, highlighting oviENs (SMP550) and Earmuff neurons (CB0550).
(J) Input neurons to oviENs.

Figure 2. Activation of Earmuff is sufficient to subtract value from an egg-laying option
(A) Image of SkinnerSys hardware to administer light to 40 individual flies in closed loop.
(B) Light delivery scheme administered by SkinnerSys. Top: when the fly is away from the light-baited side ("NL", to the left of the software-designated pink line), light is withheld. Bottom, when the fly crosses over the pink line to the "L" side, light is triggered. P: plain agarose. Red fill denotes activation of red LEDs.
(C) Actual images depicting what was described in panel **B**. Note that the light appears dim because of a filter we placed in front of the cameras (see Methods).
(D) Representative image of the egg-laying preferences of 12 *Earmuff>CsChrimson* flies when given two plain options, one of which baited with light.
(E) PIs for control (n = 52) and *Earmuff>CsChrimson* flies (n = 54) in the light-versus-no-light task.
(F) Numbers of eggs laid by control (n = 41) and *Earmuff>CsChrimson* (n = 40) flies in the light-on-both-sides task. $p = 0.1320$. Note: see Methods for details on the statistical analyses on all comparisons performed in this study.

Figure 3. Earmuff neurons are an indirect target of the sweet taste neurons and differentially activated by the superior (plain) and inferior (sucrose) substrates
(A) (False-colored) confocal image showing the morphology of Earmuff in the brain.
(B) (False-colored) confocal image showing the of morphology TPN2 in the brain. Note that the somas of these neurons are in the ventral nerve cord (VNC).
(C) Genetically Reconstituted Across Synaptic Partners (GRASP) signals (green puncta) demonstrating direct physical contacts between Earmuff and TPN2 in the SEZ (yellow rectangle).

(D) Left: schematic of substrate presentation to the legs of a fly during *in vivo* brain imaging. Right: temporal sequence of substrate presentation: a sucrose substrate (150 mM sucrose in 1% agarose) and a plain substrate (1% agarose) are presented alternately. Each presentation lasts ~ 60 seconds, with ~ 30 seconds in between.
(E) Responses of Earmuff (n = 10) to sucrose and plain substrates. Solid line: mean; shaded areas: 95% CI. Orange and green bars below the plot indicate contacts with the sucrose and plain substrates, respectively, and this illustration is used for similar plots throughout the manuscript. **(E')** Left: area under the curve (AUC) of Earmuff responses (n = 10) to sucrose vs. plain substrates. Note that each dot on the plot represents a response averaged from three technical replicates. Right: AUC of Earmuff responses (n = 10) to plain substrate vs. plastic surface. The choice for using AUC for Earmuff is because its response tends to sustain.
(F) Responses of TPN2 (n = 10) to sucrose vs. plain substrates. **(F')** Left: maximum (max) response of TPN2 (n = 10) to sucrose vs. plain substrates. Right: max response of TPN2 (n = 5) to plain substrate vs. plastic surface.

Figure 4. The strength of sucrose rejection varies among different wild-caught strains and is governed by relatively simple genetic control
(A) World map showing the locations (red stars) where some the assayed strains were collected.
(B) PI of the strains originally collected at the locations shown in panel **A**.
(C) PI of parental strains (w^{1118}/w^{1118} and *51/51*) and their F1 progeny ($w^{1118}/51$). Sample sizes: n = 111, 113 and 149.
(D) PI of parental strains (*128/128* and *51/51*) and their F1 progeny (*128/51*). Sample sizes: n = 58, 48, and 64.

Figure 5. SNP analysis of F_2 hybrids between laboratory WT and an African strain identified variations in the regulatory region of *pumillo* (*pum*) as potentially important for the trait
(A) Crossing scheme to generate F2 hybrids between w^{1118} and *51*.
(B) PIs of sample F_2 recombinant flies we processed. The flies we sent out for full-genome sequencing were somewhat different.
(C) A high-level description of the GWAS approach we used to identify candidate genes.
(D) Genomic location and annotated isoforms of *pum*, with three relevant SNPs marked with orange vertical lines. (Two of the SNPs are only 7 bp apart.) All three SNPs are located in introns.
(E) Relative *pum* expression in brains of *51/51* vs. $51/w^{1118}$ (control) and brains of in *51/pum* vs. w^{1118}/pum (control). Gene expression levels were normalized to *actin5C*. Statistical significance was assessed using a one-sample t-test against 0. Each circle represents comparison of one biological repeat of "mutant" vs. one biological repeat of control. Sample sizes: n = 11 and 8.
(F) Complementation of different *pum* alleles with *51*. Sample sizes: n = 111, 112, 182, and 44.

Figure 6. Earmuff neurons' ability to differentiate between sucrose and plain substrates is reduced when *pum* expression decreases
(A, B) Responses of Earmuff in pum/w^{1118} (control, n = 21) and *pum/51* flies ("mutant", n = 21) to the sucrose (**A**) and plain (**B**) substrates.
(C, D) AUCs of the Earmuff responses of the flies from panel **A** to the sucrose (**C**) and plain (**D**) substrates.
(E) Ratios (plain vs. sucrose) of the AUCs of the Earmuff responses of the flies from panel **A**.
(F, G) Responses of TPN2 in pum/w^{1118} (control, n = 36) and *pum/51* flies (n = 32) to the sucrose (**F**) and plain (**G**) substrates.

(H, I) Max responses of TPN2 of the flies from panel **F** to the sucrose (**H**) and plain (**I**) substrates.
(J) Ratios (plain vs. sucrose) of the max responses of TPN2 of the flies from panel **F**.

Figure 7. Cell-autonomous *pum* reduction or *para* upregulation in the Earmuff or TPN2 neurons increases their response to the plain substrate and contributes to sucrose acceptance
(A) Left: PIs of control flies (n = 54) and flies with *pum* selectively knocked down in Earmuff (n= 36). Right: PIs of control flies (n = 72) and flies with *para* selectively overexpressed in Earmuff neurons (n = 65).
(B) Left: PIs of control flies (n = 54) and flies with *pum* selectively knocked down in TPN2 (n = 57). Right: PIs of control flies (n= 45) and flies with *para* selectively overexpressed in TPN2 (n = 47).
(C, D) Responses of Earmuff in control flies (n = 20) and flies with *pum* selectively knocked down in Earmuff to the sucrose (**C**) and plain (**D**) substrates (n = 20).
(E) AUCs of the Earmuff responses of the flies from panel **C**. Left: responses to sucrose substrate; middle: to plain substrate; right: ratios (plain vs. sucrose) of the AUCs.
(F, G) Responses of Earmuff in control flies (n = 30) and flies with *para* selectively overexpressed in Earmuff (n = 29) to the sucrose (**F**) and plain (**G**) substrates.
(H) AUCs of Earmuff responses of the flies from panel **F**. Left: responses to sucrose substrate; middle: to plain substrate; right: ratios (plain vs. sucrose) of the AUCs.
(I, J) Responses of TPN2 in control flies (n = 31) and flies with *pum* selectively knocked down in TPN2 (n = 31) to the sucrose (**I**) and plain (**J**) substrates.
(K) Max responses of TPN2 of the flies from panel **I**. Left: responses to sucrose substrate; middle: to plain substrate; right: ratios (plain vs. sucrose) of the max responses.
(L, M) Responses of TPN2 in control flies (n = 30) and flies with *para* selectively overexpressed in TPN2 (n = 30) to the sucrose (**L**) and plain (**M**) substrates.
(N) Max responses of TPN2 of the flies from panel **L**. Left: responses to sucrose substrate; middle: to plain substrate; right: ratios (plain vs. sucrose) of the max responses.

Figure 8. A model illustrating the proposed circuit basis for different decision biases in the lab WT vs. the African strain
Top: In lab WT flies, TPN2 neurons are strongly activated by the sucrose substrate, providing excitatory input to Earmuff, a GABAergic interneuron. In turn, Earmuff activation enhances suppression of oviEN and oviDN, promoting sucrose rejection. Conversely, TPN2 and Earmuff are less activated by the plain substrate, resulting in weaker inhibition of oviEN and oviDN, facilitating plain acceptance.
Bottom: In African (*51*) flies, reduced *pum* and consequently enhanced *para* expression make TPN2 and Earmuff neurons more excitable compared to WT. This increased excitability is more pronounced when flies contact the plain substrate, leading to heightened suppression of oviEN and oviDN on this substrate. As a result, the relative value of plain substrate decreases, increasing acceptance of the sucrose substrate.

Figure S1. Workflow of our automatic egg-counting tool
Our egg-counting tool detects eggs in the two agarose substrates within each arena from an image of the baseplate of our apparatus (**Figure 1**) and outputs the counts into a CSV file.
Step 1: detect the well located at the center in each arena in a picture using a neural network.
Step 2: determine the chamber type and interpolate undetected wells.
Step 3: determine the agarose areas in each arena.
Step 4: detect eggs on the agarose areas using a second neural network.
Step 5: convert the numbers of eggs detected in each arena to a tabular format.

Figure S2. Earmuff dampens the response of oviEN and oviDN to sucrose solution
(A) Response of oviEN in control flies (n = 26) and flies with Earmuff neurons inhibited by tetanus toxin (TNT) (n = 28) to 150 mM sucrose solution. The arrow indicates the time at which flies' legs are exposed to sucrose solution.
(B) Maximum responses of oviEN of the flies from panel **A**.
(C) Response of oviDN in control flies (n = 17) and flies with Earmuff neurons inhibited by TNT (n =16) to sucrose solution. The arrow indicates the time at which flies' legs are exposed to sucrose solution.
(D) Maximum responses of oviDN of the flies from panel **C**.

Figure S3. TPN2 neurons are a direct postsynaptic target of the leg sweet neurons
(A) Confocal image of TPN2 neurons labeled by *ss66351* (green). The brain and ventral nerve cord (VNC) are stained with NC82 (red), a neuropil marker. Axonal termini can be seen at both SEZ and SLP.
(B) Confocal image showing some of the TPN2 neurons have axons terminated only at the SEZ. These neurons were isolated via randomly labeling subsets of neurons labeled by *ss66351* using the FLP-out approach. Arrow points to the SLP area.
(C) Confocal image showing the GRASP signals between TPN2 and *Gr5a*-expressing sweet neurons in the T1 (arrow), T2, and T3 regions of the VNC.
(D) Confocal image showing the neurons intersected by *TPN2-LexA* and *ss66351*.
(E) PIs of control flies (n = 85) and flies whose TPN neurons intersected by *TPN2-LexA* and *ss66351* (n = 96) were selectively inhibited.
(F) Response of TPN2 neurons to a sucrose solution (n = 8). The arrow indicates when flies' legs were exposed to the solution.
(G) Response of TPN2 neurons (n = 2 flies, 2-3 technical repeats) to optogenetic stimulation of *Gr64f*-expressing sweet neurons. Stimulation consisted of 5 × 10 ms red LED pulses at 50 Hz. The arrow indicates the onset of stimulation.

Figure S4. Earmuff neurons respond to sucrose exposure of the legs and optogenetic sweet neuron activation
(A) Responses of Earmuff neurons to a 150 mM sucrose solution (n = 8) and a 150 mM sorbitol solution (n = 5). The arrow indicates when flies' legs were exposed to the solution.
(A') Max responses of Earmuff of the flies from panel **A**.
(B) Responses of Earmuff neurons to optogenetic stimulation in control flies (n = 5) and in flies expressing *CsChrimson* in their *Gr5a* neurons (n = 5). Stimulation period (shaded area): 5 × 10 ms pulses of red LED at 50 Hz. To protect the PMT from the LED light, a mechanical shutter was closed during stimulation.

Figure S5. The response of Earmuff to sucrose substrate depends on functional TPN2
(A) Confocal image showing the localization of Synaptotagmin (Syt), a presynaptic marker, in processes of TPN2 within the SEZ when Syt is overexpressed in TPN2.
(B) Confocal image showing the localization of Syt in processes of Earmuff within the SLP when Syt is overexpressed in Earmuff.
(C) Responses of Earmuff to sucrose substrate in control animals (n = 12) and flies with synaptic output of TPN2 inactivated (n = 9). Note that inactivating the synaptic output of Earmuff with TNT (in *control>TNT* animals) did not affect their Ca^{2+} response in the soma of Earmuff.
(D) AUCs of the Earmuff responses of the flies from panel **C**.

Figure S6. Impact of sex and mating status on the response properties of Earmuff and TPN2
(A-C) Confocal images showing the morphology of Earmuff (green) in the brains (red) of mated females, virgin females, and males.
(D) Confocal image of GRASP signals (green) between TPN2 and Earmuff in the SEZ region of the brain.
(E, F) Responses of Earmuff in mated (n = 13) and virgin females (n = 13) to sucrose (**E**) and plain (**F**) substrates.
(G, H) Responses of Earmuff in mated females (n = 10) and males (n = 11) to sucrose (**G**) and plain (**H**) substrates.
(I, J) Responses of TPN2 in mated (n = 16) and virgin females (n = 16) to sucrose (**I**) and plain (**J**) substrates. Max responses were used for comparison.
(K, L) Responses of TPN2 in mated females (n = 10) and males (n = 10) to sucrose (**K**) and plain (**L**) substrates. Max responses were used for comparison.
(M) Ratios (plain vs. sucrose) of the AUCs of the Earmuff responses of the flies from panels **E-H**.
(N) Ratios (plain vs. sucrose) of the max responses of TPN2 of the flies from panels **I-L**.

Figure S7. Response of Earmuff and TPN2 in different genetic backgrounds
(A) Responses of the same Earmuff neurons as in **Figure 6A** when sucrose and plain substrates were presented alternately. The alternate presentation was done for all panels in this figure.
(B) Responses of the same Earmuff neurons as in **Figure 7C**.
(C) Responses of the same Earmuff neurons as in **Figure 7F**.
(D) Responses of the same TPN2 as in **Figure 6F**.
(E) Responses of the same TPN2 as in **Figure 7I**.
(F) Responses of the same TPN2 as in **Figure 7L**.

Figure S8. Complementation tests among three additional wild-caught strains
(A) PIs for line 53 (n = 39), line128 (n = 58), line 51 (n = 48), and their F1 progeny (n = 64).
(B) PIs for line 04 (n = 63), line 51 (n = 70), and their F1 progeny (n =84).
(C) PIs for line 04 (n = 117), line 128 (n = 90), and their F1 progeny (n = 76).
(D) PIs for line 42 (n = 71), line 51 (n = 77), and their F1 progeny (n = 90).
(E) PIs for line 42 (n = 85), line 128 (n = 82), and their F1 progeny (n = 94).
(F) Reduction of *pum* expression in the heads of line 51 and line 128 against control (line 53). Gene expression levels were normalized to *actin5C*.

Table S1. List of additional SNPs associated with increased sucrose acceptance of line 51

Fig. 1

A

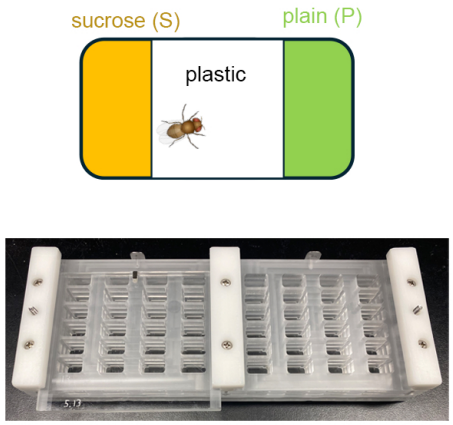

A'

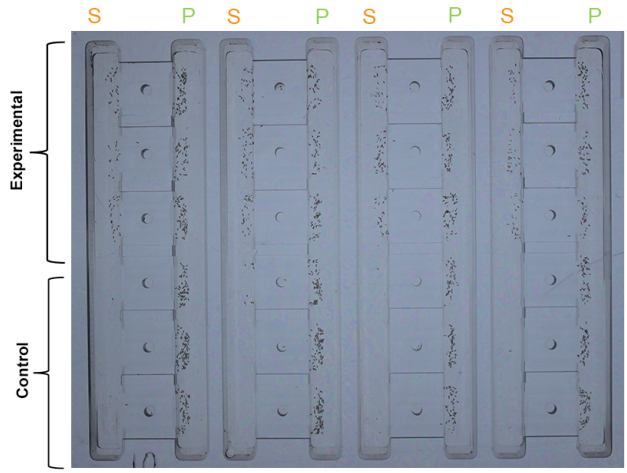

A"

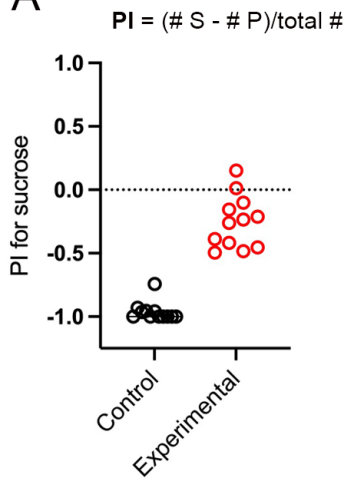

Neuron silencing screen

B

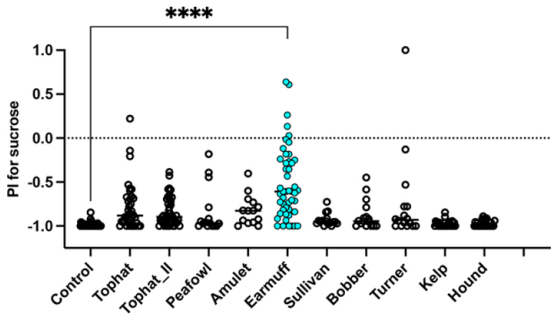

Retest

C

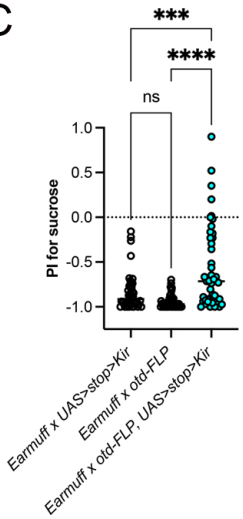

D

Earmuff>GFP

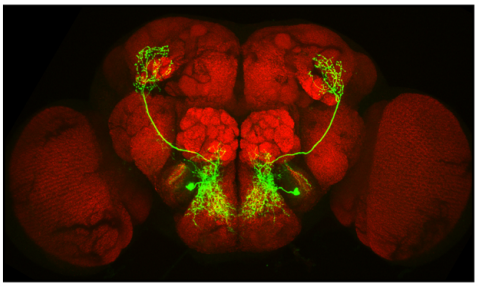

E

Earmuff ∩ vGAT>GFP

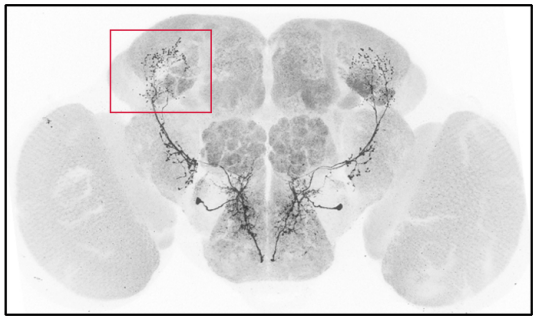

F

Earmuff>GFP

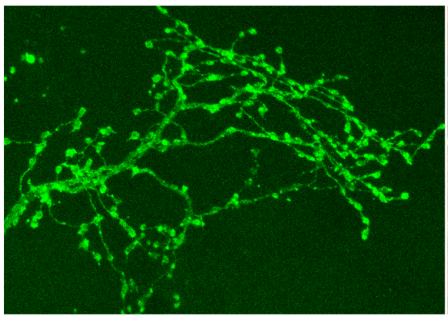

G

Earmuff>GFP, vGAT

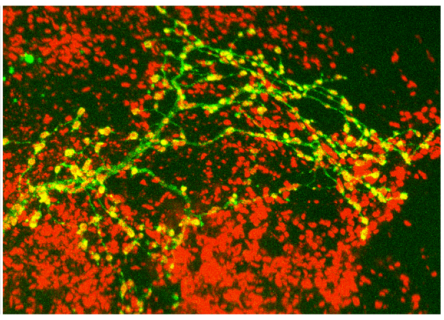

H

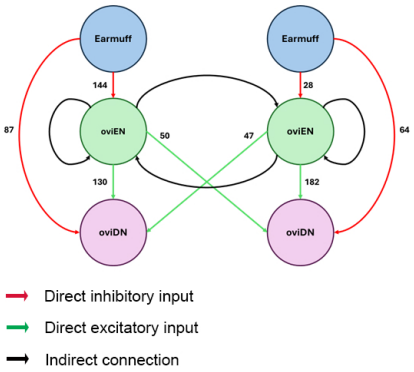

I

Inputs to oviDN

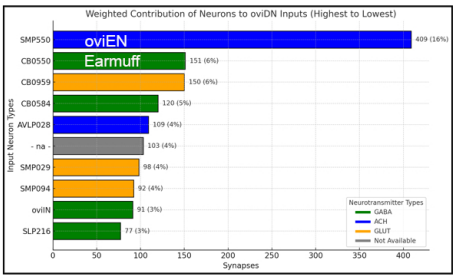

J

Inputs to oviEN

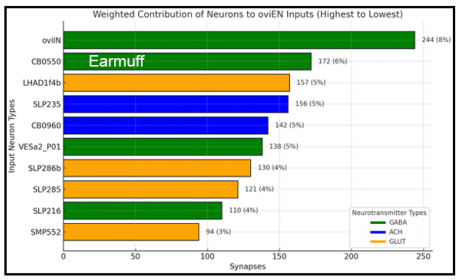

Fig. 2

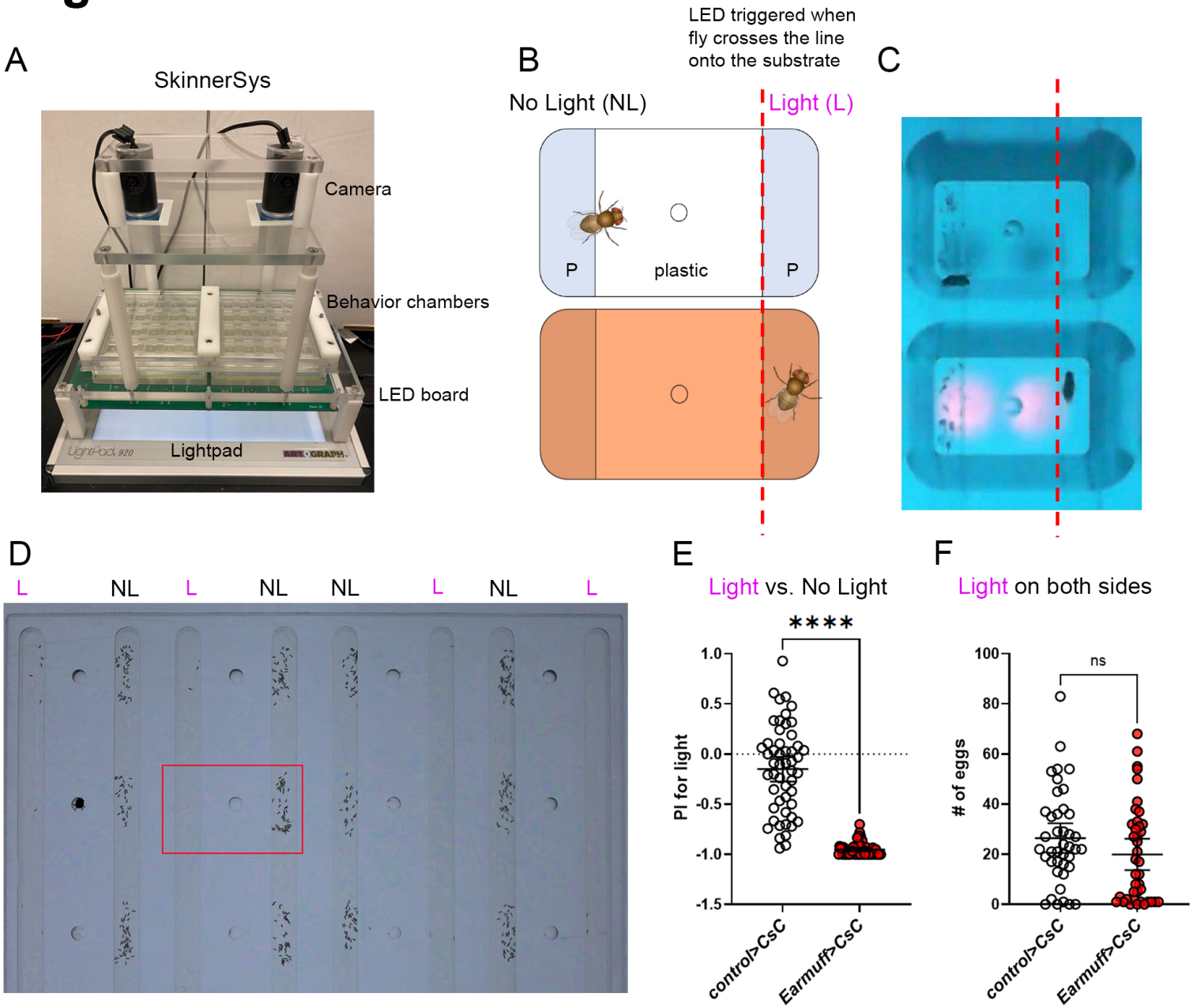
A
SkinnerSys
Camera
Behavior chambers
LED board
Lightpad
B
LED triggered when fly crosses the line onto the substrate
No Light (NL)
Light (L)
P
plastic
P
C
D
L
NL
L
NL
NL
L
NL
L
E
Light vs. No Light
****
PI for light
1.0
0.5
0.0
-0.5
-1.0
-1.5
control>CsC
Earmuff>CsC
F
Light on both sides
ns
# of eggs
100
80
60
40
20
0
control>CsC
Earmuff>CsC

Fig. 3

Earmuff>tdTomato | *TPN2>tdTomato* | GRASP between *TPN2* and *Earmuff*

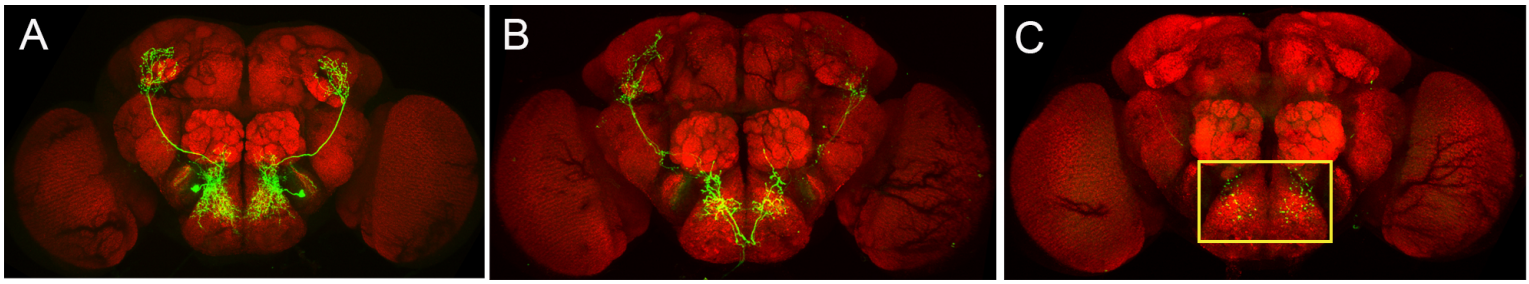

D

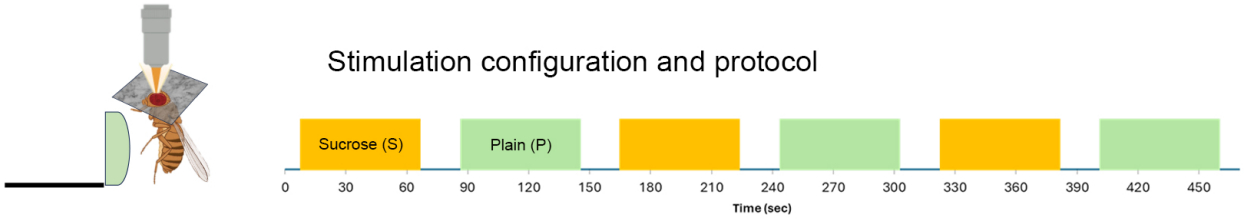

E

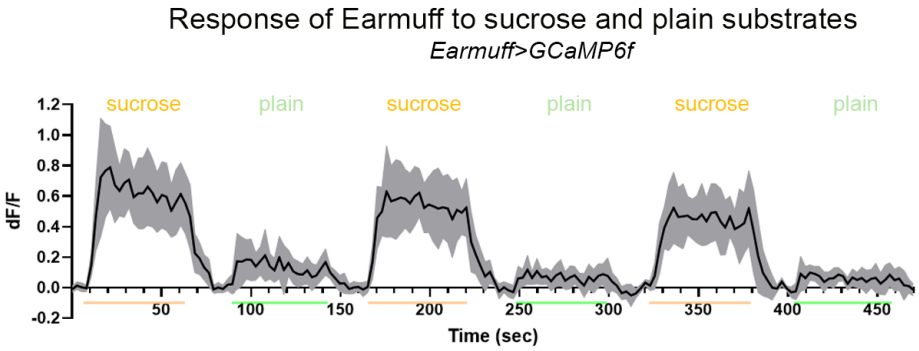

E'

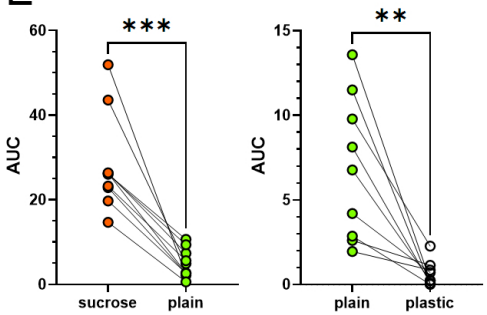

F

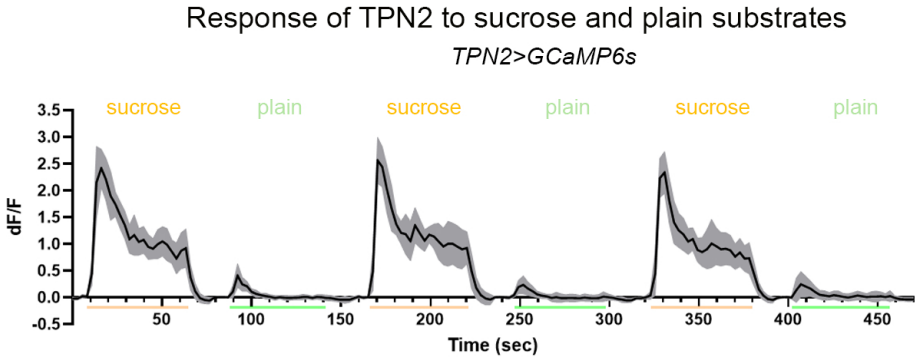

F'

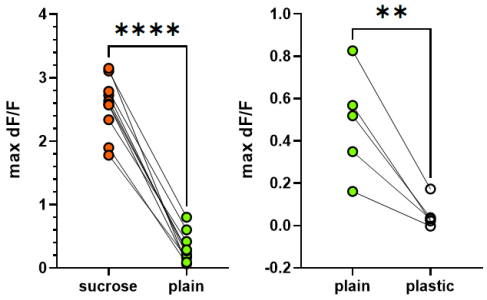

Fig. 4

A

Locations where the lines were isolated

B

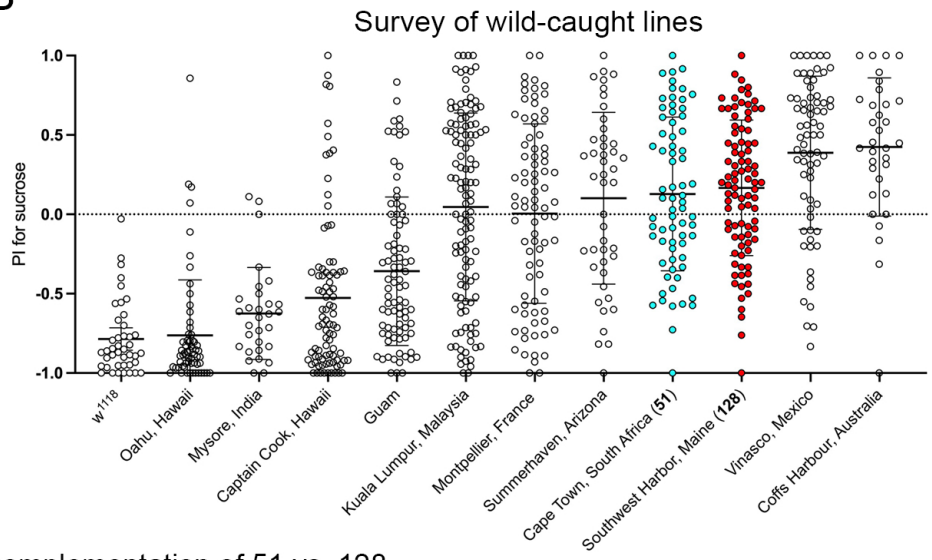

C

Complementation of 51 vs. w^{1118}

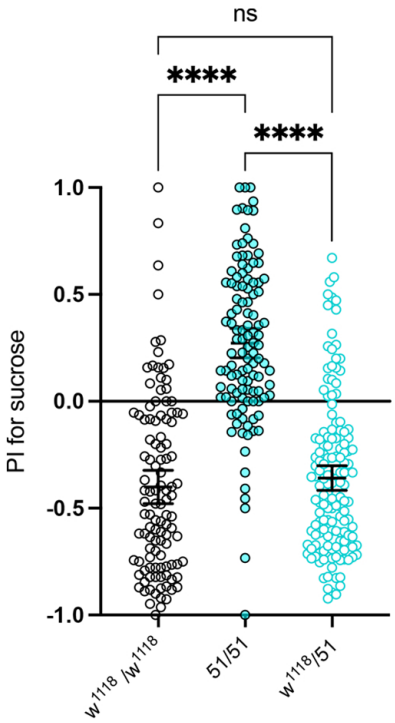

D

Complementation of 51 vs. 128

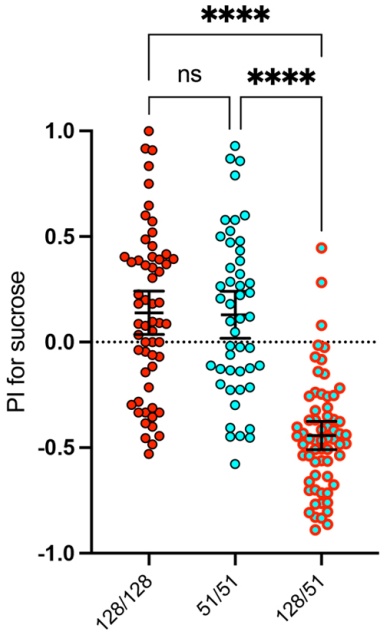

Fig. 5

A

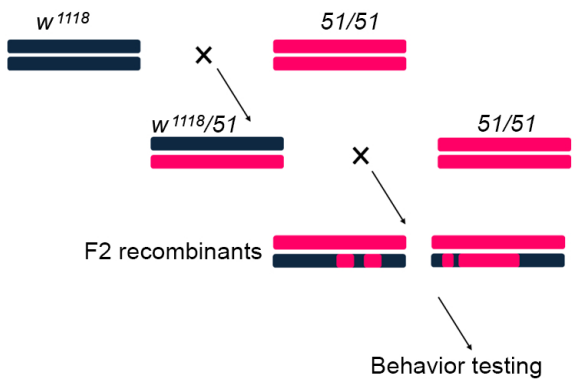
Crossing scheme
w 1118
51/51
w 1118/51
51/51
F2 recombinants
Behavior testing

B

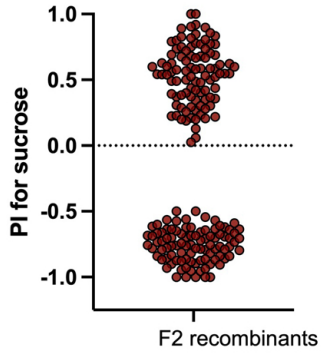
PI of sample F2 recombinants
PI for sucrose
1.0
0.5
0.0
-0.5
-1.0
F2 recombinants

C

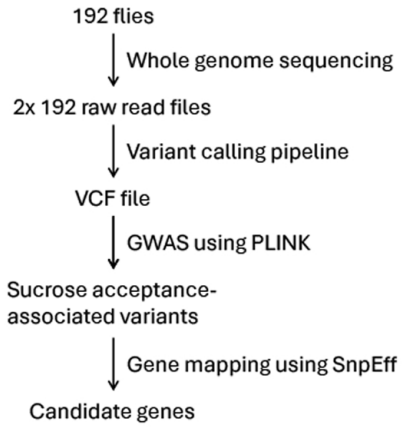
Identification of candidates
192 flies
Whole genome sequencing
2x 192 raw read files
Variant calling pipeline
VCF file
GWAS using PLINK
Sucrose acceptance-associated variants
Gene mapping using SnpEff
Candidate genes

D

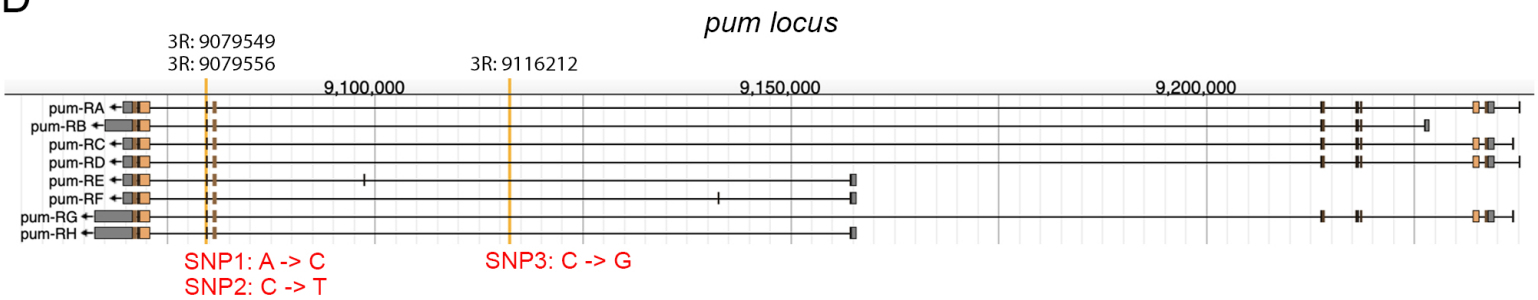
pum locus
3R: 9079549
3R: 9079556
3R: 9116212
9,100,000
9,150,000
9,200,000
pum-RA
pum-RB
pum-RC
pum-RD
pum-RE
pum-RF
pum-RG
pum-RH
SNP1: A -> C
SNP2: C -> T
SNP3: C -> G

E

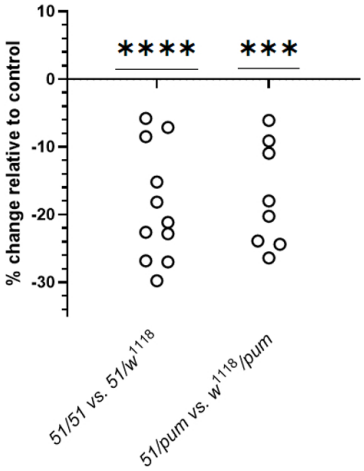
RT-qPCR
(brains)
% change relative to control
10
0
-10
-20
-30
****
***
51/51 vs. 51/w 1118
51/pum vs. w 1118 /pum

F

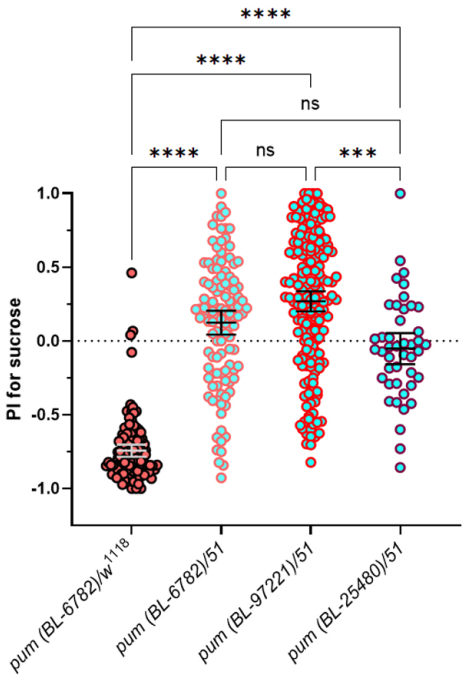
Complementation of 51 vs. pum
PI for sucrose
1.0
0.5
0.0
-0.5
-1.0
****
****
ns
****
ns
***
pum (BL-6782)/w 1118
pum (BL-6782)/51
pum (BL-97221)/51
pum (BL-25480)/51

Fig. 6

Response of Earmuff to plain and sucrose substrates
(*Earmuff>GCaMP8m*)

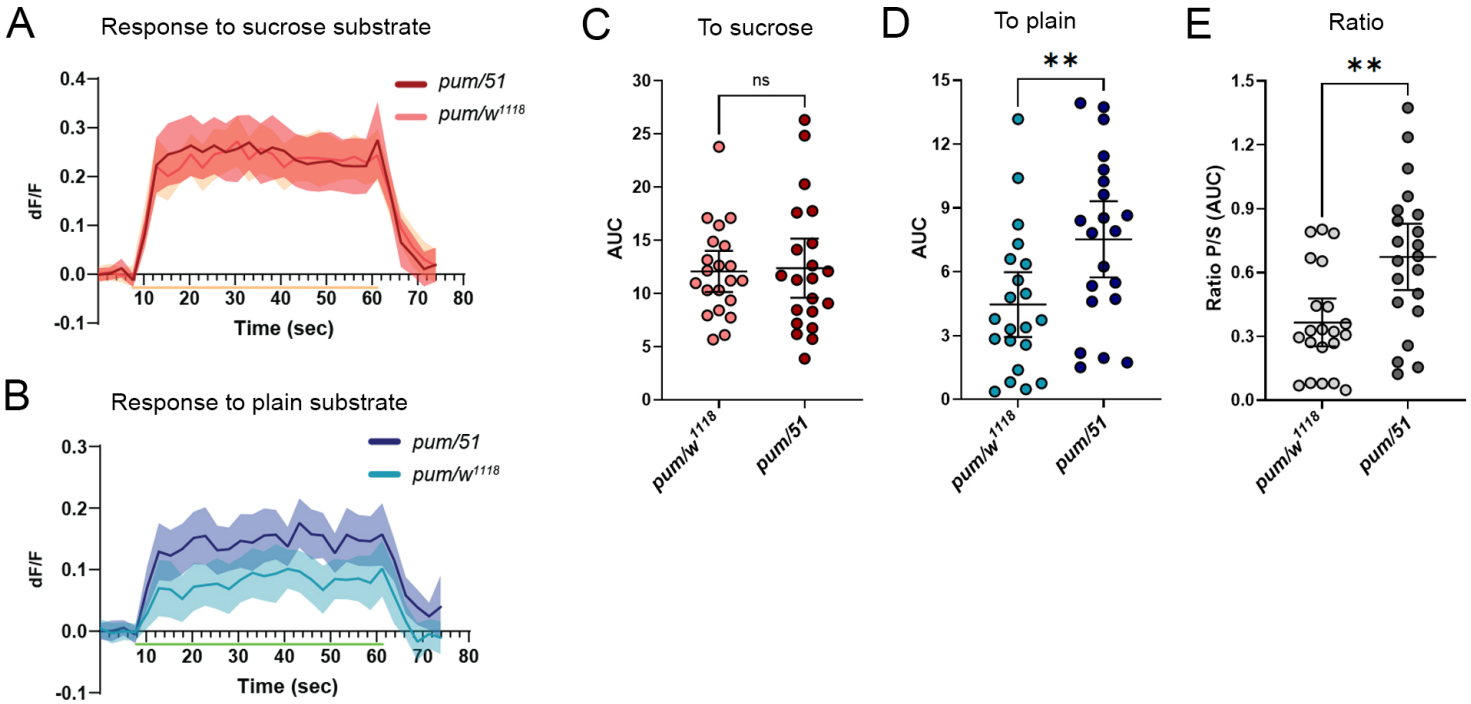

Response of TPN2 to plain and sucrose substrates
(*TPN2>GCaMP6s*)

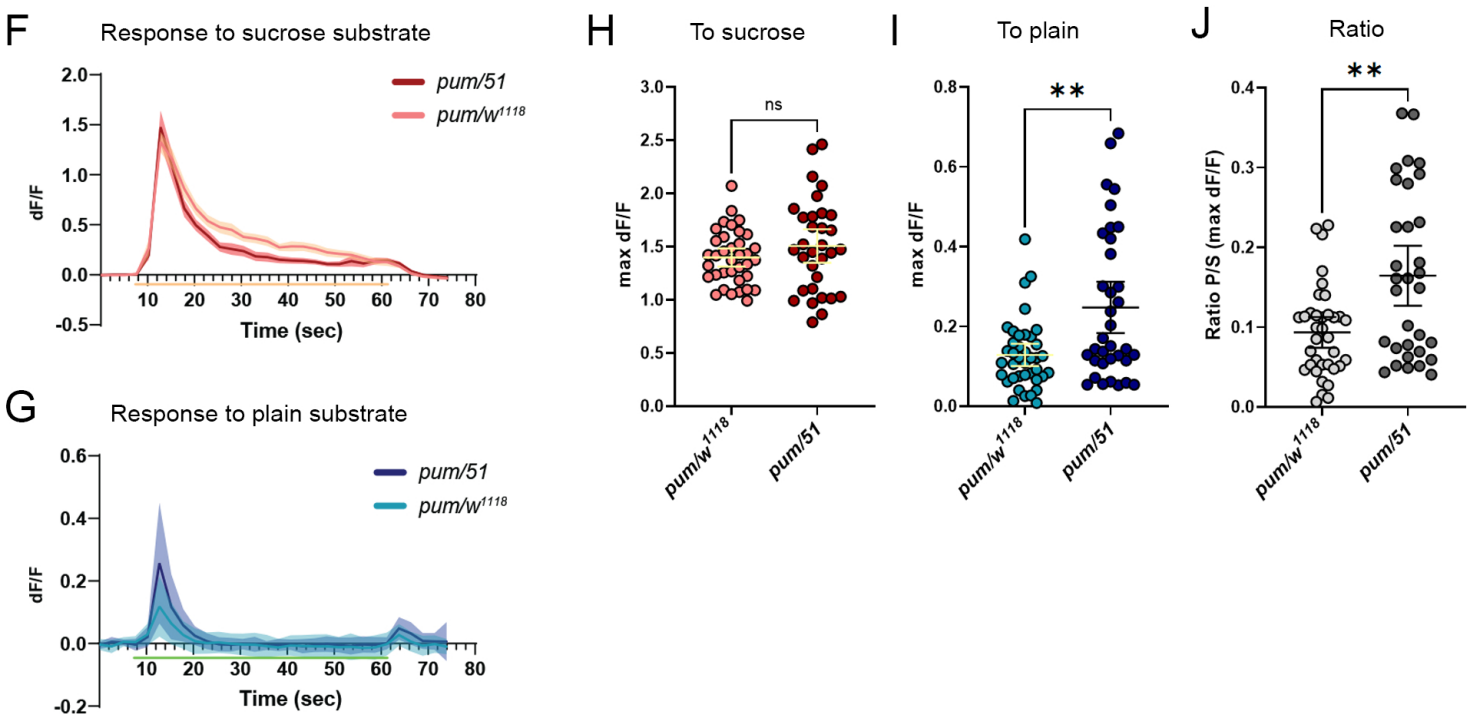

Fig. 7

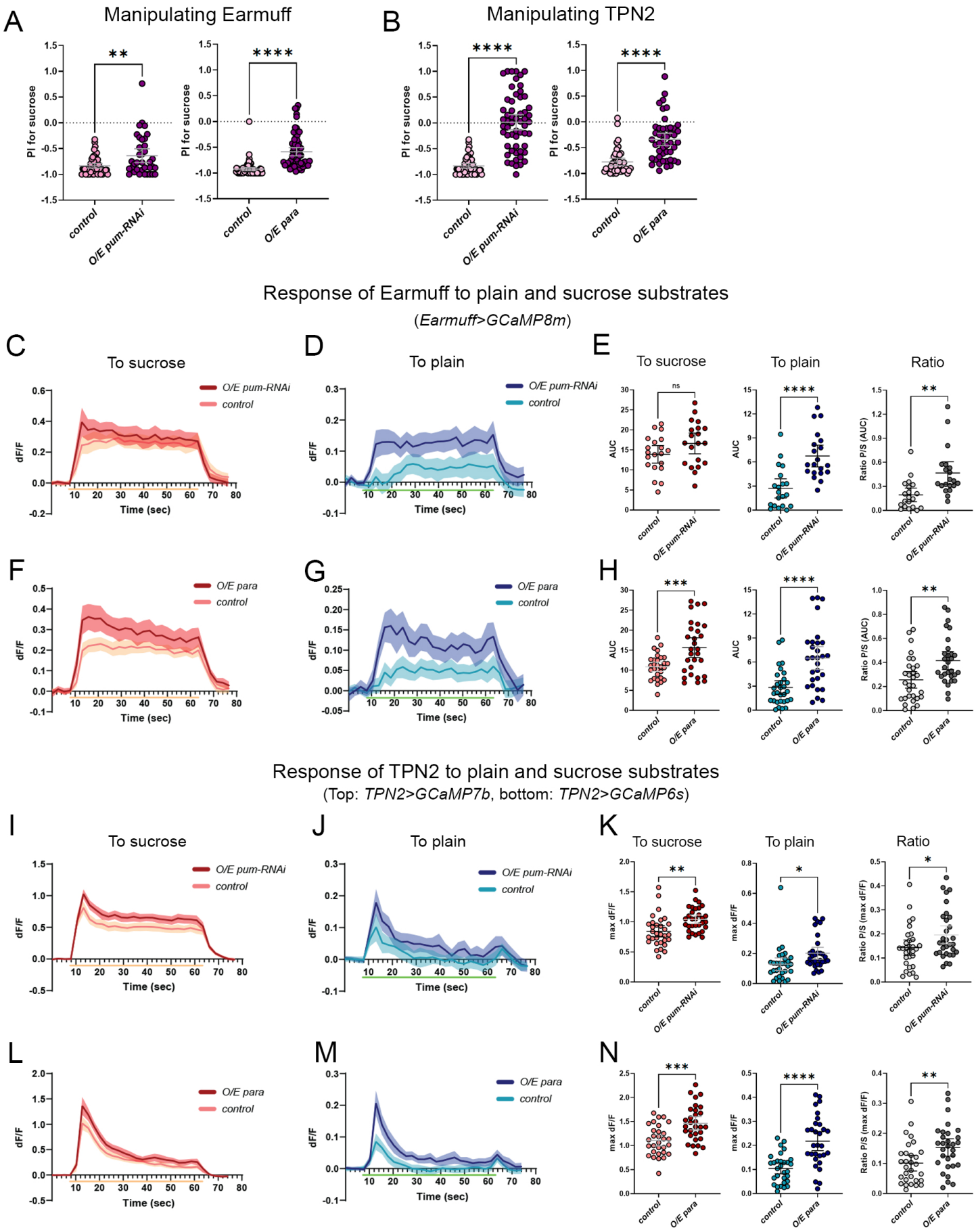
A
Manipulating Earmuff
B
Manipulating TPN2
PI for sucrose
control
O/E pum-RNAi
O/E para
Response of Earmuff to plain and sucrose substrates
(Earmuff>GCaMP8m)
C
To sucrose
D
To plain
E
To sucrose
To plain
Ratio
F
G
H
Response of TPN2 to plain and sucrose substrates
(Top: TPN2>GCaMP7b, bottom: TPN2>GCaMP6s)
I
J
K
L
M
N
dF/F
Time (sec)
AUC
Ratio P/S (AUC)
max dF/F
Ratio P/S (max dF/F)
ns

Fig. 8

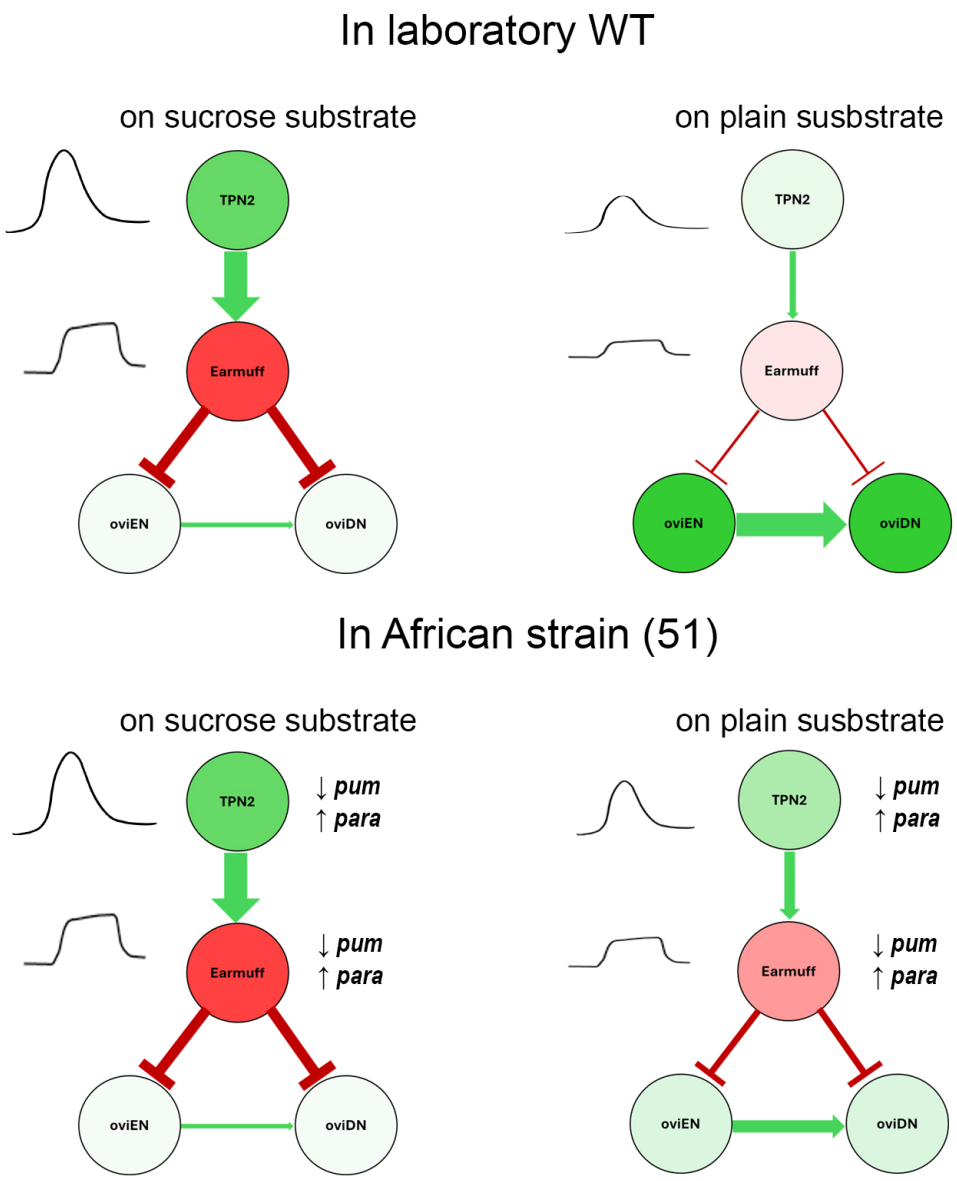
In laboratory WT
on sucrose substrate
on plain susbstrate
TPN2
Earmuff
oviEN
oviDN
TPN2
Earmuff
oviEN
oviDN
In African strain (51)
on sucrose substrate
on plain susbstrate
TPN2
↓ pum
↑ para
Earmuff
↓ pum
↑ para
oviEN
oviDN
TPN2
↓ pum
↑ para
Earmuff
↓ pum
↑ para
oviEN
oviDN

Figure S1

Upload egg-laying image

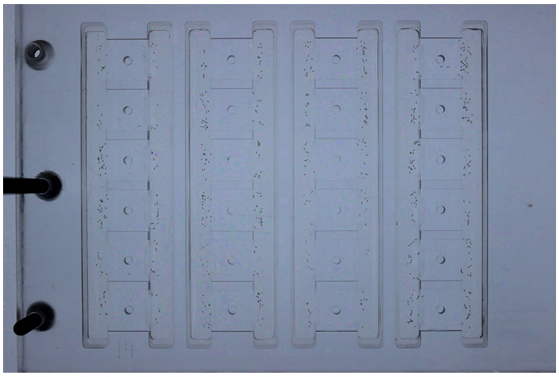

1

Detect arena wells via neural network

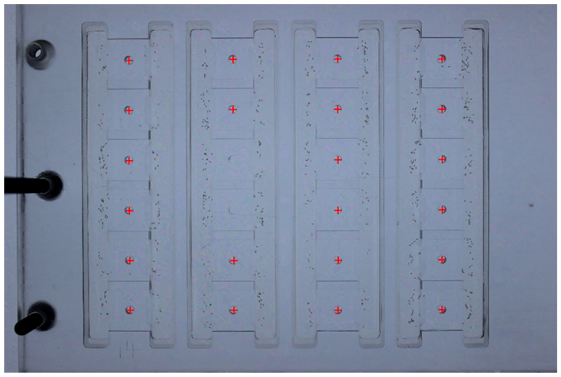

2

Determine chamber type & interpolate undetected wells

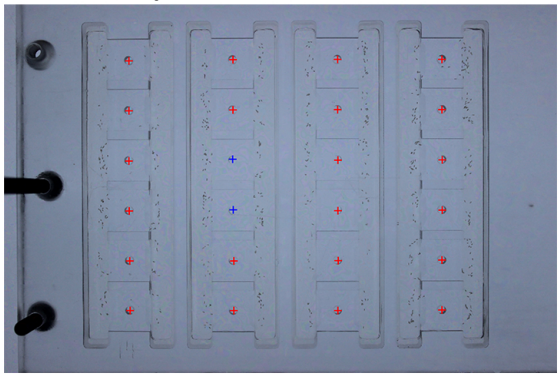

3

Determine agarose positions

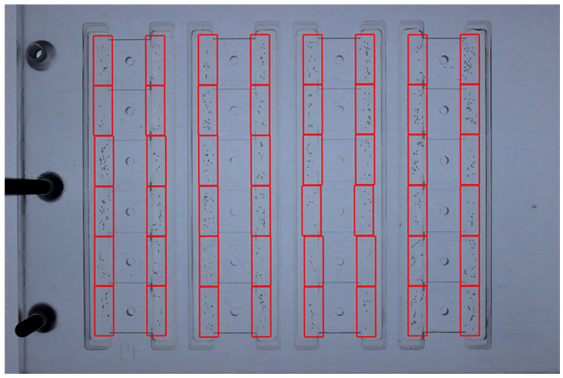

4

Detect eggs via neural network

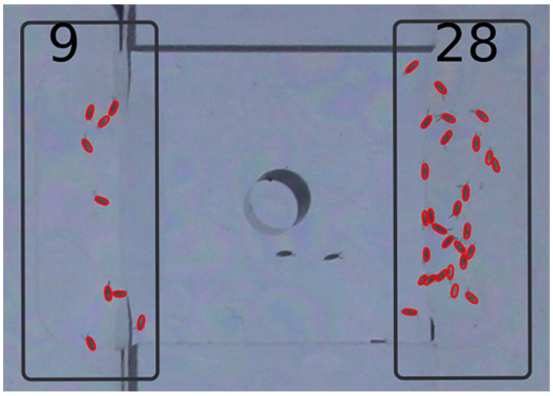

5

Convert egg counts to tabular format

	A	B	C	D	E	F	G	H
1	Egg Counter (model v2021-11-09)							
2	14_left.JPG							
3								
4	11	7	10	12	14	21	9	28
5	7	5	23	10	12	19	18	21
6	23	7	14	14	12	15	23	13
7	23	17	21	21	6	9	13	12
8	8	10	13	10	7	2	15	20
9	13	6	12	15	9	8	23	20

Fig. S2

Response of oviEN to sucrose solution w/ and w/o input from Earmuff

A

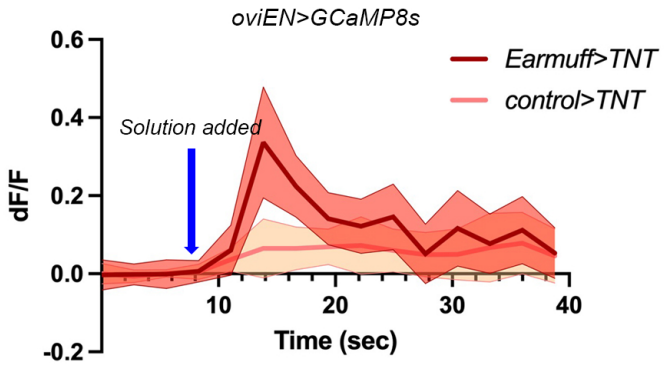

B

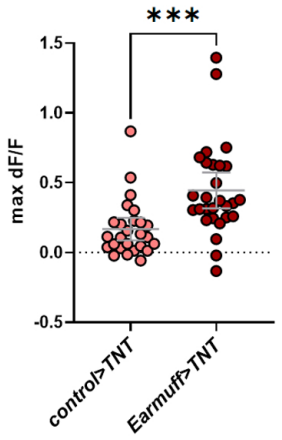

Response of oviDN to sucrose solution w/ and w/o input from Earmuff

C

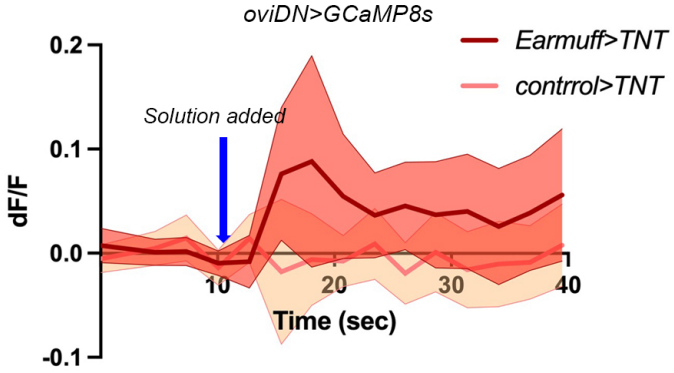

D

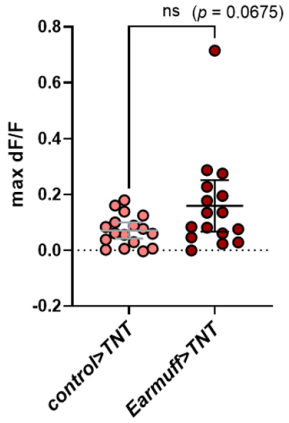

Fig. S3

A

TPN2-ss-GAL4>GFP

B

TPN2-ss-GAL4>GFP
"flipped-out clone"

C

GRASP between *Gr5a* and *TPN2*

D

TPN2-lexA ∩TPN2-ss-GAL4>GFP

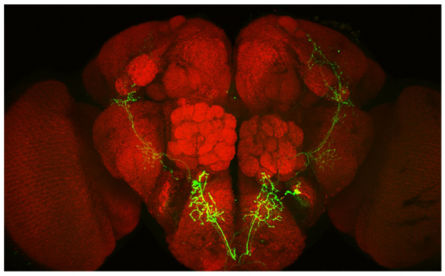

E

TPN2-lexA ∩TPN2-ss-GAL4>Kir2.1

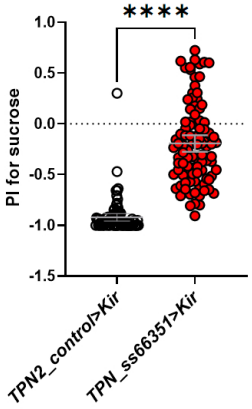

F

TPN2>GCaMP6s

Sucrose solution

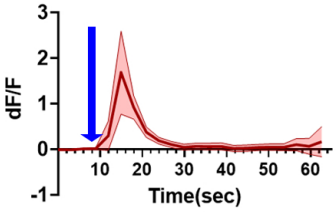

G

TPN2>GCaMP6s

Opto sugar

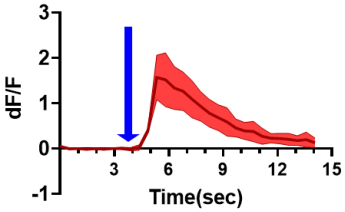

Fig. S4

Response of Earmuff to sugar solutions

A

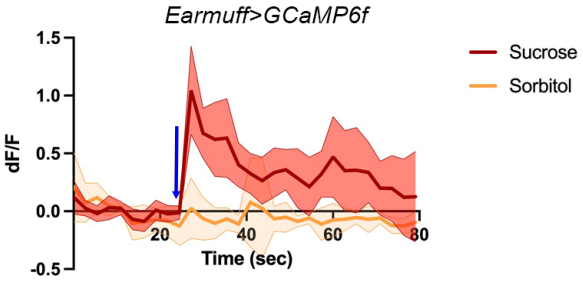

A'

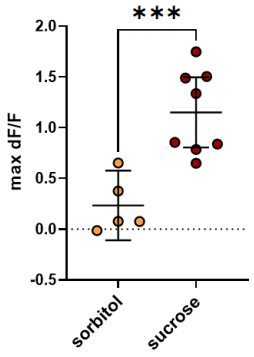

B

Response of Earmuff to "opto sugar"

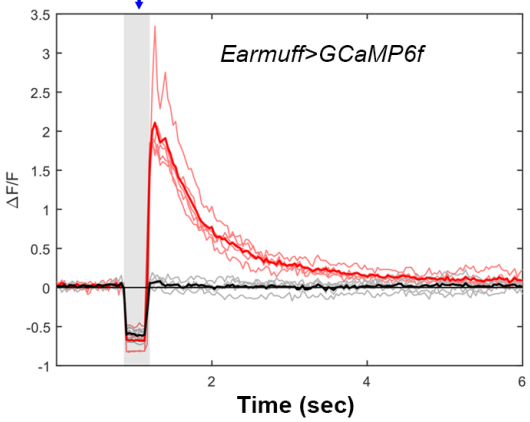

Fig. S5

A

TPN2>syt

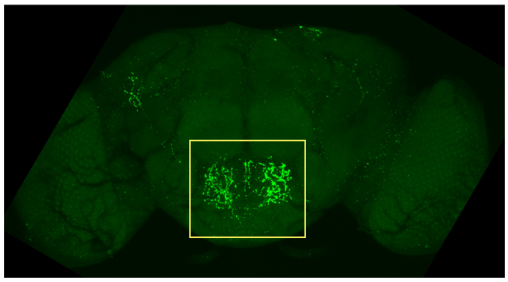

B

Earmuff>syt

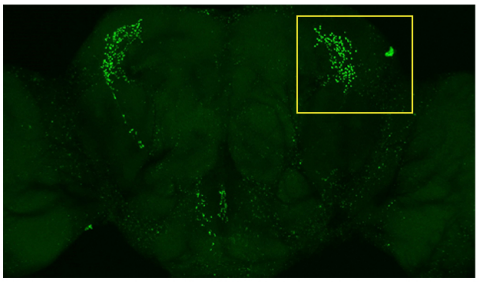

Response of Earmuff to sucrose substrate

C

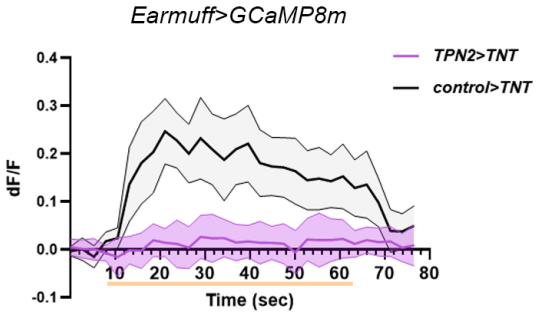

D

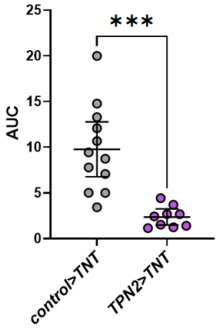

Fig. S6

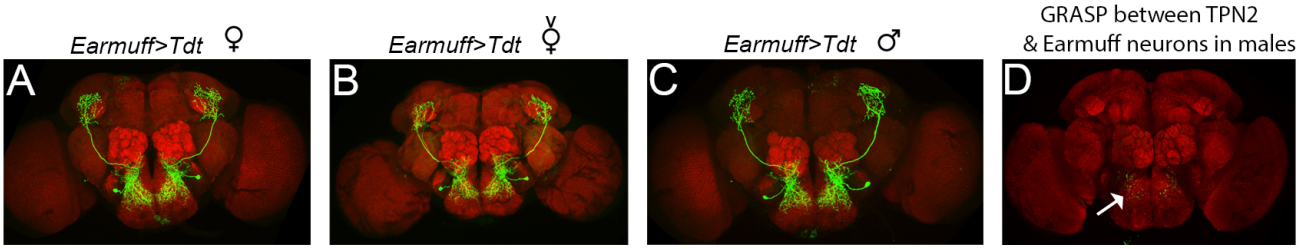
Earmuff>Tdt ♀
Earmuff>Tdt ♀
Earmuff>Tdt ♂
GRASP between TPN2 & Earmuff neurons in males
A
B
C
D

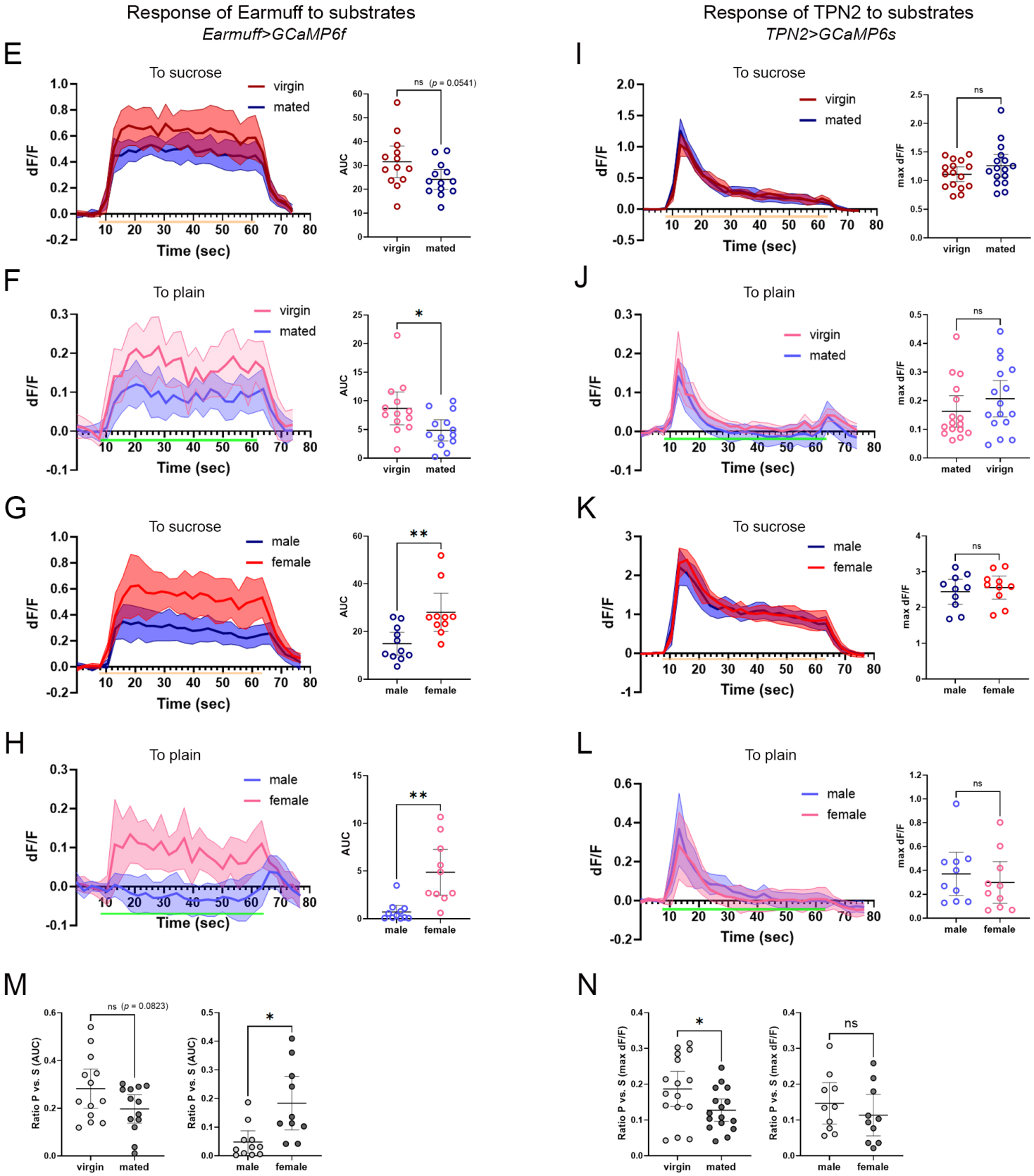
Response of Earmuff to substrates
Earmuff>GCaMP6f
Response of TPN2 to substrates
TPN2>GCaMP6s
E
To sucrose
virgin
mated
dF/F
Time (sec)
AUC
ns (p = 0.0541)
I
To sucrose
max dF/F
ns
F
To plain
*
J
To plain
G
To sucrose
male
female
**
K
To sucrose
H
To plain
L
To plain
M
Ratio P vs. S (AUC)
ns (p = 0.0823)
N
Ratio P vs. S (max dF/F)
ns

Fig. S7

Response of Earmuff to substrates in different genetic backgrounds

Earmuff>GCaMP8m

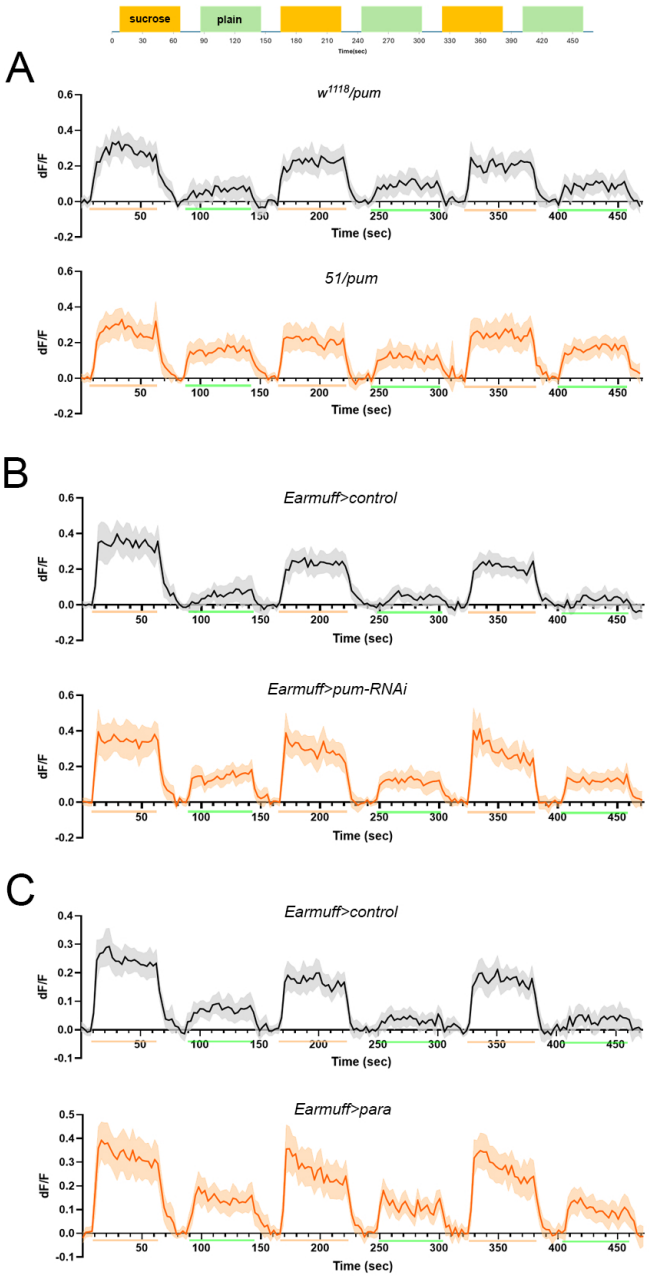

Response of TPN2 to substrates in different genetic backgrounds

TPN2>GCaMP6s and 7b

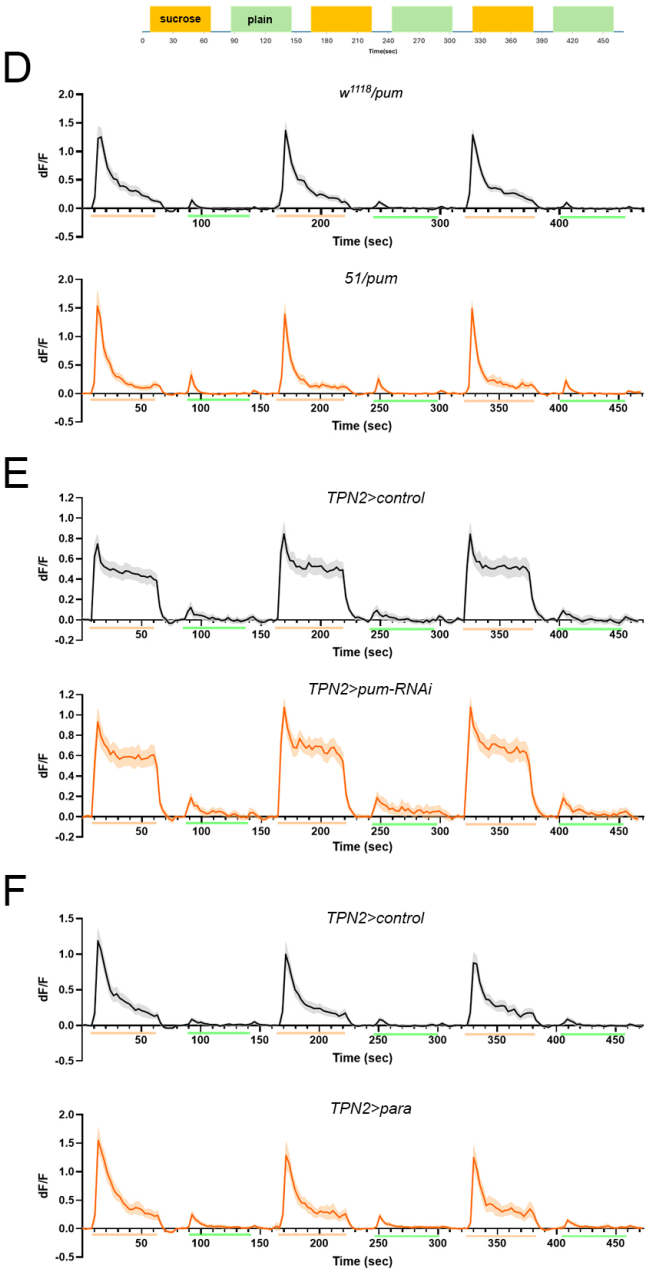

Fig. S8

51: South African
128: Maine
04: Malaysia
42: Mexico
53: Mauritius

Complementation tests

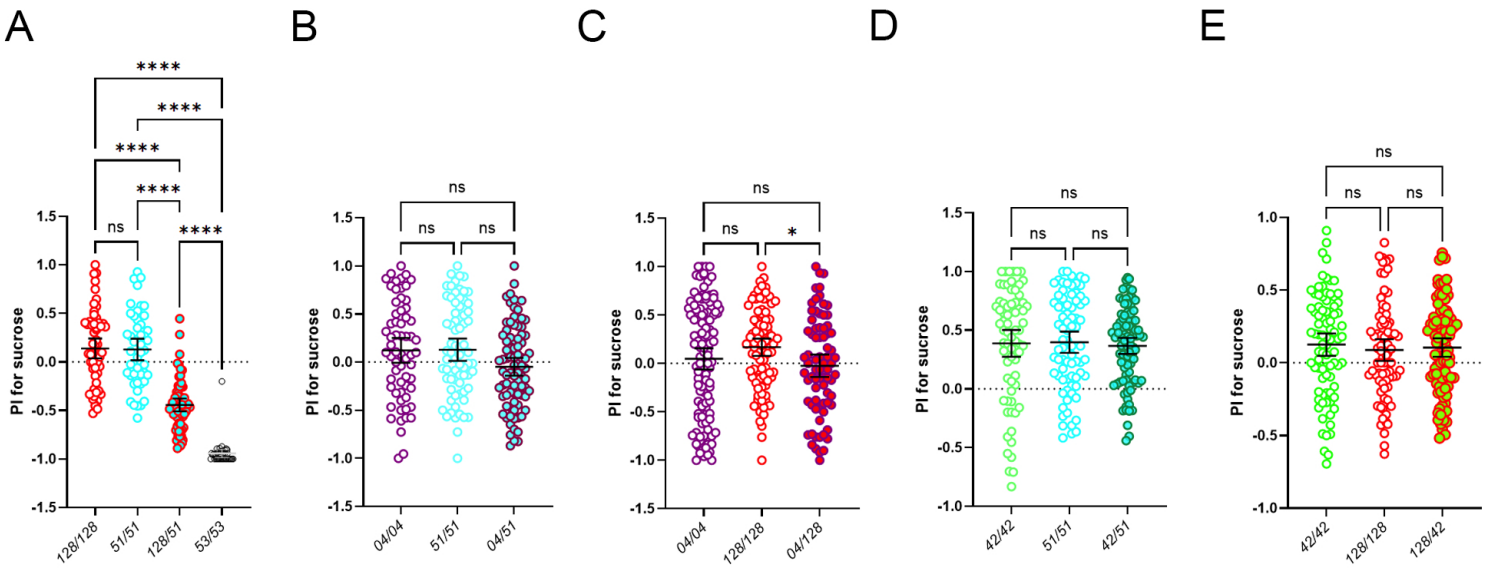

F

RT-qPCR (heads)

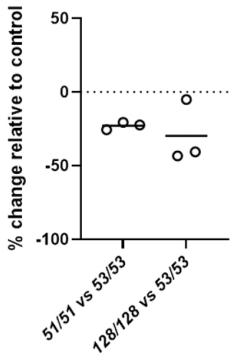

Table S1

Variant		Genotype distribution by phenotype group		Potentially affected genes
Position	**Seq. change**	**PI ≥ -0.1**	**PI ≤ -0.75**	
3L:14590265	T->G	0/13/25	0/56/8	HGTX (intron)
3L:15778514	C->A	0/13/32	0/61/17	lncRNA:CR46197-CG6244 (intergenic_region)
3L:16013248	G->A	0/6/30	0/48/19	lncRNA:CR43950 (downstream), lncRNA:CR45998 (upstream), mib1 (upstream), mib1-lncRNA:CR43950 (intergenic_region)
3L:16013253	GCA->G	0/6/36	0/48/25	lncRNA:CR43950 (downstream), lncRNA:CR45998 (upstream), mib1 (upstream), mib1-lncRNA:CR43950 (intergenic_region)
3L:16047436	ATATG->A	0/11/34	0/57/17	Diap1 (intron,upstream), Mbs (upstream), asRNA:CR45889 (downstream), lncRNA:CR43951 (upstream)
3L:18147732	A->T	0/14/33	1/59/15	CG7330 (upstream), geko (downstream), geko-CG7330 (intergenic_region)
3L:18147735	C->A	0/14/33	1/59/15	CG7330 (upstream), geko (downstream), geko-CG7330 (intergenic_region)
3L:25627853	A->AGGTGTTTAC...	0/13/32	0/61/16	RR48317_transposable_element (upstream), lovit (intron)
3R:8107261	C->CA	0/15/28	0/61/10	CG7900 (downstream), FBti0019335 (upstream), puc (intron)
3R:9079556	C->T	0/14/23	0/60/5	pum (intron)
3R:11019925	*->ATGT	0/12/32	0/59/15	side-VI (intron)
3R:11831160	TTC->T	1/16/30	0/64/11	CG6959 (intron)
3R:12966855	T->C	0/14/32	0/64/15	CG14384 (intron,upstream), CG7381 (downstream), Cyp304a1 (downstream), Spc25 (downstream), grsm (intron)
3R:13868303	*->T	4/11/28	30/28/14	E5 (intron), lncRNA:CR46239 (upstream)
3R:14968498	T->G	0/14/31	0/60/13	FBti0062141-lncRNA:CR45599 (intergenic_region)
3R:15125530	T->G	0/14/33	1/58/14	CG42788 (intron)
3R:15783287	*->ACATGTG	4/11/22	31/27/9	CG5614 (downstream), CG5614-CG9590 (intergenic_region), CG9590 (upstream)
3R:18634603	CAAAAAAAAA...->C	0/6/34	0/44/18	CG14301 (intron), qin (intron)
3R:25532557	TC->*	3/12/21	31/25/12	msi (intron)